$\mathcal{TWIST}$: Research Proposal

Executive Summary

- Using data taken and analyzed in the past two years, the $\mathcal{TWIST}$ collaboration has demonstrated the feasibility of realizing a substantial improvement in muon decay parameter measurements. In so doing, we have improved the precision on ρ and δ by factors of 2.5 and 2.9 respectively, representing the first improvements on the numbers for decades. These results also lead to a significant improvement in precision for $\mathcal{P}_\mu\xi$.
- The analysis strategy was validated by this first phase of physics measurements, and is ready for the next phase.
- We have realistically assessed systematic uncertainties in detail, and believe that we understand how they can be controlled and minimized.
- The eventual goal of $\mathcal{TWIST}$ is to improve all three parameters by at least one order of magnitude compared with previous experiments; for $P_\mu\xi$, we are confident of twice that.
- All the tools are in place for continuing toward the final goals of the experiment: the detector, the analysis software, the simulation, the computing resources, and very importantly, the manpower. Expertise in the issues of data collection, simulation, and analysis is now in place, and we must capitalize on this.

1 Introduction

$\mathcal{TWIST}$, the TRIUMF Weak Interaction Symmetry Test, is in the process of measuring the parameters describing the energy and angle (with respect to muon spin) distributions of positrons (e^+) from positive muon (μ^+) decay. These muon decay parameters, or Michel parameters (after Prof. L. Michel [1]), offer a compact and convenient prediction of the electroweak interaction in muon decay. They can be related to a more recent description in terms of coupling constants for interactions of muons and electrons of definite handedness [2].

This proposal describes the methods by which we measure the Michel parameters. We have already increased the experimental precision for the ρ [3] and δ [4] parameters by factors of 2.5 and 2.9 respectively, and are now in the process of further improving these results at the same time as we make our first measurement of $P_\mu\xi$. The eventual goal of $\mathcal{TWIST}$ is to improve all three parameters by at least one order of magnitude compared with previous experiments; for $P_\mu\xi$, we are confident of twice that. We also plan to establish an independent measurement of the η parameter as well; whether it will be competitive with a dedicated PSI experiment [5] remains to be seen.

In addition, we discuss the physics motivation and the significance of the collaboration's objectives, and show what we have learned about the challenges to be faced in the minimization of the different sources of systematic errors. It summarizes the recent progress we have made as a group toward our objectives, and how our students and research associates contribute to the tasks involved.

2 Physics Motivation

The Standard Model of the strong, weak and electromagnetic interactions, based on the gauge group $SU(3)_C \times SU(2)_L \times U(1)_Y$, has proven to be remarkably successful in describing the existing experimental observations. At present, there exist no experimental results that deviate from its expectations, with the exception of neutrino oscillations which in any case result from a simple extension to the mass matrices. However, the Standard Model is universally believed to be an incomplete theory of nature in spite of its many successes, and many extensions have been proposed.

Normal muon decay $\mu \to e\nu\overline{\nu}$ is a process which is exceptionally well suited to studies of the space-time structure of the weak interaction. This comes about because the purely leptonic nature of the decay eliminates many uncertainties due to the internal structure of the particles or to contributions from other interactions.

By assuming a completely general, local, derivative-free, lepton-number-conserving, four-fermion point interaction, the matrix element for muon decay can be written in the charge-changing form as [2, 6]:

$$M = \frac{4G_F}{\sqrt{2}} \sum_{\substack{\gamma=S,V,T \\ \varepsilon,\mu=R,L}} g^{\gamma}_{\varepsilon\mu} \langle \bar{e}_{\varepsilon} | \Gamma^{\gamma} | (\nu_e)_n \rangle \langle (\bar{\nu}_{\mu})_m | \Gamma_{\gamma} | \mu_{\mu} \rangle \tag{1}$$

This includes scalar, vector, and tensor ($\Gamma^S, \Gamma^V, \Gamma^T$) interactions among charged lepton spinors of definite chirality ($\varepsilon, \mu = R$ or L). There are 10 complex amplitudes $g^{\gamma}_{\varepsilon\mu}$ (g^T_{LL} and g^T_{RR} are zero), resulting in 19 independent real parameters. In the Standard Model, $g^V_{LL} = 1$ and all others are zero (a $V-A$ interaction). Constraints on the values of the coupling constants are derived from observables.

Under the same assumptions, neglecting neutrino masses and radiative corrections, averaging over the polarization of the decay e^+, the differential decay rate of the positive muon is expressed as [1, 7, 8]

$$\frac{d^2\Gamma}{dx\ d\cos\theta} = \frac{1}{4} m_{\mu} W^4_{\mu e} G^2_F \sqrt{x^2 - x_0^2}\ \{\mathcal{F}_{IS}(x) + \mathcal{P}_{\mu} \cos\theta \cdot \mathcal{F}_{AS}(x)\} \tag{2}$$

where

$$W_{\mu e} = \frac{m_{\mu}^2 + m_e^2}{2m_{\mu}} \qquad \mathcal{P}_{\mu} = |\vec{\mathcal{P}}_{\mu}|$$

$$x = \frac{E_e}{W_{\mu e}} \qquad \cos\theta = \frac{\vec{\mathcal{P}}_{\mu} \cdot \vec{p}_e}{|\vec{\mathcal{P}}_{\mu}|\,|\vec{p}_e|}$$

$$x_0 = \frac{m_e}{W_{\mu e}}$$

The isotropic and asymmetric parts, respectively, in the decay rate are written in terms of the decay (Michel) parameters ρ, η, δ, and ξ.

$$\mathcal{F}_{IS}(x) = x(1-x) + \frac{2}{9}\rho(4x^2 - 3x - x_0^2) + \eta x_0 (1-x) \tag{3}$$

$$\mathcal{F}_{AS}(x) = \frac{1}{3}\xi\sqrt{x^2 - x_0^2}\left[1 - x + \frac{2}{3}\delta\left\{4x - 3 + \left(\sqrt{1 - x_0^2} - 1\right)\right\}\right] \tag{4}$$

$$\tag{5}$$

Radiative corrections to the distribution are substantial, and must be incorporated. Corrections have been calculated including full $O(\alpha)$ radiative corrections with exact electron mass dependence,

leading and next-to-leading logarithmic terms of $O(\alpha^2)$, leading logarithmic terms of $O(\alpha^3)$, corrections for soft pairs, virtual pairs, and an ad-hoc exponentiation [9, 10, 11]. The result is adequate for measurements with a precision better than 10^{-3}, and higher order estimates, motivated by the sensitivity of $\mathcal{TWIST}$, can be performed.

The Standard Model predicts the decay parameters to take the values $\rho = \frac{3}{4}$, $\eta = 0$, $\delta = \frac{3}{4}$, and $\xi = 1$. The actual values of the parameters are very sensitive to the Standard Model assumption that the interaction is pure left-handed vector $(V-A)$; if terms with other characteristics are present, the parameters differ. These decay parameters, and combinations of them, can be written in terms of bilinear combinations of the more general and fundamental coupling constants $g^{\gamma}_{\varepsilon\mu}$, such that deviations from Standard Model values will place very model independent limits on the individual couplings.

Fetscher *et al.* [2] expressed the relationship in terms of probabilities $Q_{\varepsilon\mu}$ $(\varepsilon, \mu = R, L)$ for a μ handed muon to decay into a ε handed electron:

$$Q_{\varepsilon\mu} = \frac{1}{4}|g^S_{\varepsilon\mu}|^2 + |g^V_{\varepsilon\mu}|^2 + 3(1-\delta_{\varepsilon\mu})|g^T_{\varepsilon\mu}|^2$$

To demonstrate how the Michel parameters can be used in a model independent test for handedness of the muon coupling, the probability for a right-handed muon coupling can be written as:

$$\begin{aligned} Q^{\mu}_R &\equiv Q_{RR} + Q_{LR} \\ &= \frac{1}{4}|g^S_{LR}|^2 + \frac{1}{4}|g^S_{RR}|^2 + |g^V_{LR}|^2 + |g^V_{RR}|^2 + 3|g^T_{LR}|^2 \\ &= \frac{1}{2}[1 + \frac{1}{3}\xi - \frac{16}{9}\xi\delta] \end{aligned} \tag{6}$$

The Review of Particle Physics [6] summarizes the best measurements prior to $\mathcal{TWIST}$:

$$\rho = 0.7518 \pm 0.0026 \tag{7}$$
$$\eta = -0.007 \pm 0.013 \tag{8}$$
$$\delta = 0.7486 \pm 0.0026 \pm 0.0028 \tag{9}$$
$$\mathcal{P}_{\mu}\xi = 1.0027 \pm 0.0079 \pm 0.0030 \tag{10}$$
$$\mathcal{P}_{\mu}\frac{\xi\delta}{\rho} > 0.99682 \tag{11}$$

The first publications from $\mathcal{TWIST}$ [3, 4] reduce the uncertainties in ρ and δ by factors of 2.5 and 2.9 respectively. In combination with Eq. 11 and the positive semidefinite expression of Eq. 6, the value of $\mathcal{P}_{\mu}\xi$ is significantly constrained as well (see Section 5.2). The main goal of $\mathcal{TWIST}$ is to search for new physics through more precise measurements of the muon decay parameters. We aim to set new limits on the right-handed coupling of the muon in a model independent way, as well as to squeeze the parameter space for classes of extensions to the Standard Model, such as those invoking left-right symmetry, with less model dependence than otherwise possible.

Left-right symmetric (LRS) models include a heavier partner to the standard W boson which has right handed coupling. Mixing of the two bosons of mass M_L and M_R, with angle ζ, leads to small deviations of ρ and ξ from the Standard Model values

$$\frac{3}{4} - \rho = \frac{3}{2}\zeta^2 \tag{12}$$
$$\frac{1 - P_{\mu}\xi}{4} = \zeta^2 + \frac{M_L^4}{M_R^4} + \zeta\frac{M_L^2}{M_R^2} \tag{13}$$

A model which incorporates a nonlocal tensor interaction, motivated in part by results on weak radiative pion decay, leads to a modification of the Michel form and an independent parameter, κ [12].

If such a parameter was not zero, the effect on the decay spectrum shape would be a correlation with δ such that $\delta = \frac{3}{4}(1 - 6\kappa^2)$.

Other extensions to the Standard Model can be tested by $\mathcal{TWIST}$ results. Quantitative examples will be given in Section 5.

3 The $\mathcal{TWIST}$ Spectrometer

The $\mathcal{TWIST}$ detector is described in detail in [13]. This section is only a summary of that article, with the inclusion of extra information on the muon source.

The spectrometer detector consists of a symmetric array of planar detectors, called the detector stack, which is constructed to very high precision with attention paid to minimizing the amount of material in the tracking region. At the center of the array is a thin target in which the muons stop. This allows very precise measurement of positron decay tracks while minimizing interactions which would broaden and distort the detector response function. The planar geometry means that the energy loss, which depends on the length of a track in any material in its path, has a simple $1/|\cos\theta|$ dependency.

The detector stack is in a very uniform solenoidal field of 2 T. A thin scintillator records the incoming muon, providing an unbiased trigger for events. The incident beam characteristics and the beam entrance path are engineered so as to minimize depolarization, the knowledge of which is crucial in setting limits on $\mathcal{P}_\mu\xi$. At the center of the array is a thin target in which the muons stop, also chosen to minimize known sources of depolarization due to interactions of the muon with its environment prior to decay.

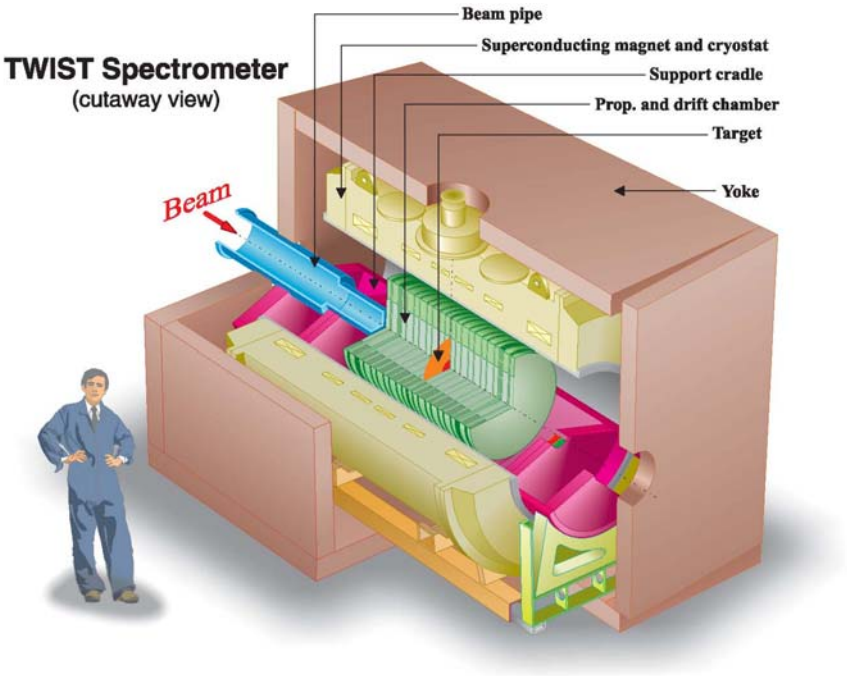

Figure 1: Conceptual drawing of the $\mathcal{TWIST}$ spectrometer. It shows the superconducting solenoid within the steel yoke, with the drift chambers and proportional chambers symmetrically placed about the central target.

A conceptual cutaway view of the spectrometer is shown in Fig. 1.

3.1 The detector array

The detector stack consists of 56 low-mass high-precision planar wire chambers, as shown in Fig. 2. $\mathcal{TWIST}$ uses two types of wire chamber detectors, which we call DCs and PCs, described in Table 1. Both types measure either the u or v coordinate, in a system rotated by $\pi/4$ from the horizontal-vertical (x, y) system.

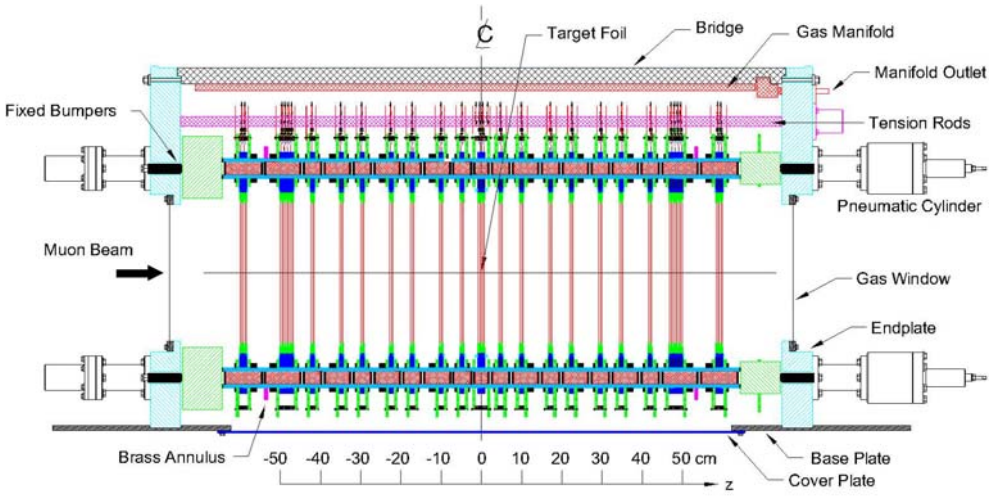

Figure 2: Side view of the symmetric $\mathcal{TWIST}$ detector stack, showing 19 modules at precise locations along the beam axis.

	Modules	Planes	Wires per plane	Wire spacing	Gas
DC	16	44	80	4 mm	DME
PC	2	8	160 $(32 + 32 \times 4)$	2 mm	CF_4/isoC_4H_{10}
PC (target)	1	4	48	2 mm	CF_4/isoC_4H_{10}

Table 1: Description of DC and PC chambers in the $\mathcal{TWIST}$ spectrometer.

The DC chambers are arranged in modules, the simplest of which is a UV module consisting of a pair of DCs, one measuring u and the other v. There are 14 of these in sparsely spaced arrays, 7 on each side of the target module. The remainder of the 44 DC modules are assembled into two densely stacked modules, at either end of the sparse arrays of UV modules. DCs use a slow gas (dimethyl ether, or DME) to achieve better position resolution. Their function is to determine precisely the coordinates of the decay positron path. The sparse arrays of UV planes near the muon stopping target (DC9-DC22 US, and DC23-DC36 DS) are spaced to minimize scattering between planes while giving some redundancy of measurement. The dense stacks of DCs (DC1-DC8 US and DC37-DC44 DS) help to resolve any pitch ambiguities in tracks.

PC chambers are also arranged in three modules. They serve to identify the primary characteristics of an event and to identify the times of each track in a window $[-6, +10]$ μs with respect to the time of a simple thin scintillator event trigger. Four PC planes in each of two modules, one at the upstream (US, PC1-PC4) and another at the downstream (DS, PC9-PC12) ends of the stack identify decay positrons; if both groups are hit, a penetrating beam positron is the likely source. Pulse widths can also be used to separate positrons from more highly ionizing tracks. Four additional PC planes (PC5-PC8) are part of the target module and surround the muon stopping target (currently 71 μm high purity Al), which acts also as a cathode for PC6 and PC7. Muons stopping in the target satisfy PC6 $\cdot$ $\overline{\text{PC7}}$.

Planes are positioned with extreme accuracy of 5×10^{-5} in the z (beam and magnetic field) direction, using specially constructed glass ceramic spacers. Alignment in the transverse u, v directions is accomplished with fits of straight tracks, but depends also on the relative wire separation accuracy which was measured with rms value of $\sigma = 3.3$ μm for 6,304 sense wires in the chamber modules (including spare modules).

Apart from the muon stopping target, the materials of the stack in the particle path are only the anode wires, 6.2 μm aluminized Mylar cathode foils defining the chamber planes, chamber gas, and He gas with a small nitrogen content in the spaces between modules. Each detector plane has a thickness of only about 5×10^{-5} radiation lengths.

Much greater detail is found in the recent submission to Nuclear Instruments and Methods, describing the detector and its construction details [13].

3.2 The solenoidal field

The nominal field of 2 T is produced by a superconducting solenoid which was originally constructed about twenty years ago as an early-generation whole body MRI field device. The vacuum enclosure has an inner diameter of 100 cm and a length of 223 cm. An external steel yoke was required to produce the required field uniformity for the detector tracking volume. It also functions to contain the return field, reducing its effect on nearby people and equipment while also reducing the influence of external changes such as the position of the building crane on the internal field. The yoke was modeled with OPERA-3d prior to fabrication. It is 20 cm thick at the top and sides, and 8 cm thick at the ends. The downstream end of the yoke is hinged for easy installation and removal of the detector cradle.

Figure 3 shows field measurements for the typical operating strength of 2.00 T. The upper plot shows the field map on the beam axis ($x = y = 0$), while the lower plot shows the field at a radius of 165 mm, at the edge of the tracking volume. Within this tracking DC volume ($|z| < 500$ mm, $r < 160$ mm), the measurements determine the variations of the field as a function of position to 5×10^{-5}. The field is uniform over the full volume to 4×10^{-3} (full width). It has also been mapped at 1.96 T and 2.04 T.

The OPERA-3d field simulation is also used to create the full field maps used for tracking and event simulation production. The measured map was made with Hall probes, only for the z component and only at discreet points. We measured at seven radii separated by 4.1275 cm, five of which are in the tracking region and two of which are beyond. The z separation interval was 5 cm; in the fringe field region near the hole in the yoke end plate through which the muon enters, where the field variation is much greater, finer steps of 1 cm were used. For a subset of points in the homogeneous tracking region, an NMR probe was also used to measure the total field, to check consistency and calibration. To reduce sensitivity to random measurement error, to improve the granularity of the map, and to supply transverse field components, the OPERA-3d map is matched and tuned to the measured Hall probe map and then used in tracking and event simulation.

In 2003, we extended the mapped region with the same device, using only five Hall probes such that the rotating arm could pass through the 40 cm diameter hole in the magnet yoke. This map overlaps the US part of the previously mapped region and extends through the hole into the fringe field region to the last quadrupole (Q7) of M13. Depolarization due to the effects of radial components in the fringe field region is important and comprises the most poorly known contribution to the total effective depolarization. Comparison with OPERA-3d has shown that it is important to include in the model the presence of the steel of the last beam line elements (Q7, Q6, and B2) of M13, and this has also been done.

In 2004, we performed detailed simulation studies on the effects of the fringe fields from the solenoid and other beam line components on the muon depolarization. The OPERA-3d model which matches the measured field map in the interior positron tracking region of the solenoid was used for the simulations. Using the beam parameters determined for the 2003 data (for a Be production target), we found an average muon polarization of 99.761(4)%. Systematic variations in the simulated muon polarization due to different assumptions in the OPERA model, such as the B-H curve of the steel and the yoke dimensions, are found to be less than 0.8×10^{-4}. This leads us to believe that, while the agreement in the upstream region for the field map and the OPERA model is not perfect, it is good enough for a measurement of $\mathcal{P}_\mu\xi$ at this level. We foresee the possible necessity of improving the map in 2005, depending on what we learn with our first direct measurement of $\mathcal{P}_\mu\xi$.

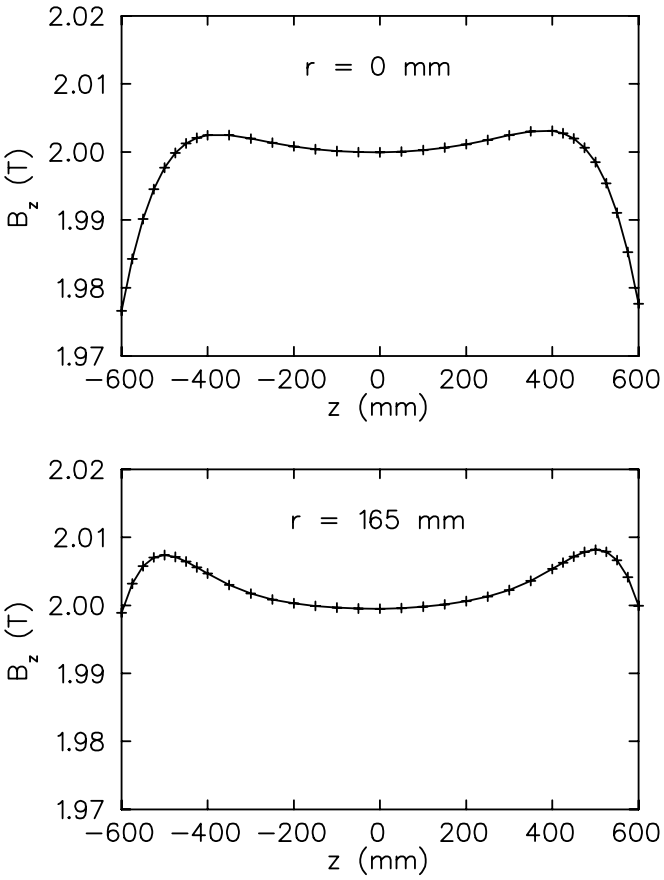

Figure 3: Maps of axial magnetic field, showing B_z vs. z for $x = y = 0$ (upper) and $r = 165$ mm (lower).

3.3 The time expansion chamber

The need for efficient and accurate characterization of the muon beam has led to the development and construction of a low-pressure, low-mass transverse drift chamber dubbed the time expansion chamber, or TEC. A depiction of the device is shown in Fig. 4. It consists of two modules, one to measure in each of the x and y directions, which are enclosed in a chamber with typically 60 torr of DME. Thin (6.25 μm) aluminized Mylar windows isolate the chamber from the beam line vacuum along the axis of the chamber. It is coupled directly into the beam line approximately half way between the last quadrupole element and the entrance to the solenoid yoke. Each of the x and y modules consists of a region of uniform transverse electric field in which the ionization drifts to 24 sense wires in multiplication regions to one side of the particle track. The time of arrival of ionization at the sense wires with respect to external detection of the beam particle (*e.g.*, by the muon trigger scintillator) determines the distance from the sense wire. Thus the position and angle of each track is measured by fitting up to 24 individual position measurements in each module.

The TEC is in a region where the fringe field of the solenoid (when it is on) is about 0.1 T, mostly in the direction of the beam particles. So far, it has been tested only in fields near zero, but we plan to use it also with the solenoid on. Even though it has very low mass, the scattering from windows, gas, and field cage wires will reduce muon polarization by scattering, so it is not anticipated to be useful while the majority of spectrometer data is being collected. However, it is made so that it can be reproducibly installed or removed in a few hours, to perform regular checks of beam position and divergence distributions. This serves to monitor systematic variations in the muon beam which will affect the precision of decay parameter measurements.

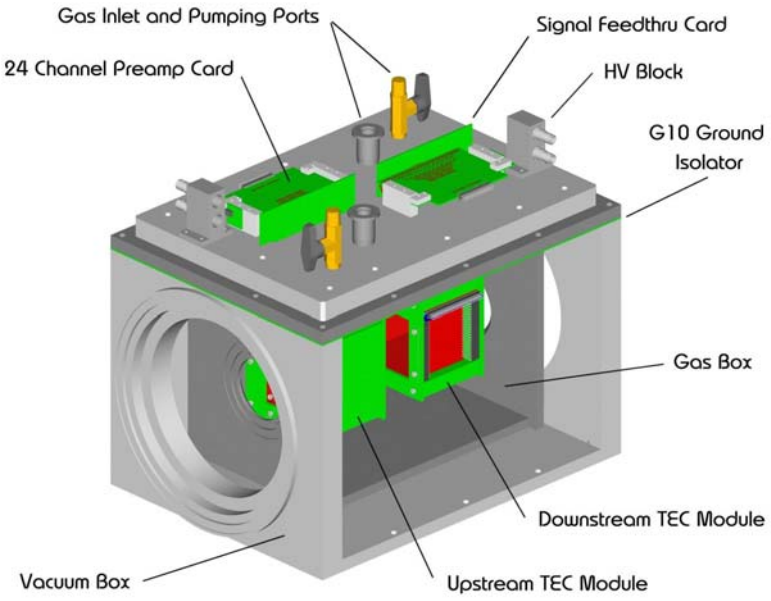

Figure 4: The TEC, showing two modules which measure the position and angle of beam particles, one in x and one in y.

An example of a beam measurement, for surface muons from a Be production target jacketed in a stainless steel water cooling jacket, is shown in Fig. 5. The irregular shape of the profile in x is due to the non-uniformity of the luminosity of the source for surface muons; the surface of the stainless steel jacket where the proton beam enters is brighter. Graphite targets are being measured in Fall 2004. They are expected to be better for both uniformity and luminosity.

3.4 The muon source

Muons for $\mathcal{TWIST}$ are produced from positive pions (π^+) decaying at rest, at or near the surface of the pion production target (surface muons). For a massless left-handed neutrino, the absence of non-Standard Model interactions leads to a positive muon (μ^+) with spin antiparallel to the momentum direction. The result is that surface muons have a high polarization in a direction opposite to the beam direction. Several factors contribute to a difference of the polarization from the ideal value. Most are controlled via a high quality, low emittance beam transport system, the M13 beam line, from the pion production target to the $\mathcal{TWIST}$ solenoid entrance.

Scattering of muons changes the momentum direction but not the spin direction, which leads to depolarization of the beam. If this happens in the high solenoidal field of the $\mathcal{TWIST}$ spectrometer, the momentum direction has already become irrelevant to the spin distribution as measured, but if it happens before entering the solenoid, it is important. By choosing muon momenta near the kinematic limit of 29.79 MeV/c, the small momentum acceptance of $\sim 1\%$ allows only very small depolarization from scattering within the pion (and muon) production target. Finite acceptance of the channel leads to a distribution of spin directions about the mean beam direction. A small and well-characterized emittance make this depolarization small and easily estimated.

Depolarization may also occur in the interactions of muons during and/or after thermalization in the muon stopping target or nearby materials. Depolarization of muons when slowing from $p = 29.8$ MeV/c down to zero is discussed in [14, 15, 16]. The effect is negligible if the incident muon has a kinetic energy of at least ~ 200 keV when it enters the solid target. Those muons that stop in the detector components may suffer depolarization, so accounting for them in the simulation is important for $P_\mu \xi$ determination. Data sets taken with the stopping distribution adjusted to favor muon stops in target PCs upstream of the stopping target can be used to assess or put limits on the depolarization,

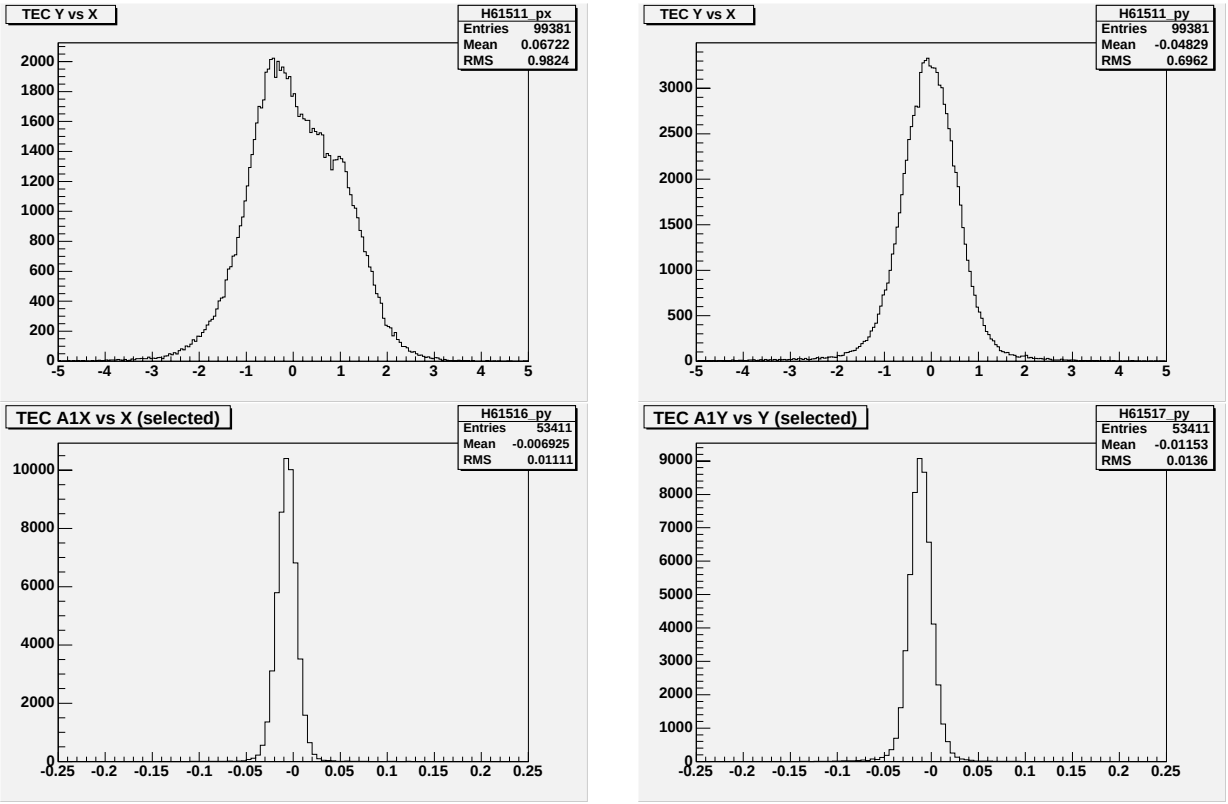

Figure 5: Projections of two-dimensional plots of a surface muon beam produced by a Be production target in a stainless steel water cooling jacket. Plotted are profiles in the x and y directions (top), and corresponding distributions of the slopes of individual muon tracks (bottom).

since we can identify unambiguously muons which stop in PC5 by the requirement PC5 $\cdot \overline{\text{PC6}}$. This depolarization is then included in the simulation to account for the small fraction of muons which stop in detectors either before or after the target.

From the positron distributions for decays after 1 μs in the graphite-coated Mylar target which was used for data taking in 2002 (see recent submissions for publication [3, 4], and Section 5.2), the mean initial polarization was estimated to be 93%, with an exponential relaxation parameter of 0.0172(5) μs^{-1}. The use of a high purity aluminum target has so far yielded a polarization roughly consistent with 100%, based on the slope of the angular distribution, but more precise estimates await the full application of the blind analysis procedure described in Section 4.

A significant potential source of depolarization for $\mathcal{TWIST}$ is the effect of the fringe field as the muon enters the solenoid. The radial field components impart transverse momentum (and spin components) to any trajectory which does not follow a field line. This can be minimized by choosing the size and divergence of the beam appropriately, and maintaining the beam exactly along the solenoid field axis. The apparent depolarization can then be reliably predicted by knowing both the beam characteristics (size, divergence, momentum, and correlations between them) and the fringe field spatial dependence. Improved information for both of these was obtained in 2003, using fast xy wire chambers in the solenoid entrance region with the solenoid field off. In 2004, the new low-mass, low-pressure beam characterization device (TEC) has been commissioned and used for the same purpose (see Section 3.3). It provides very precise information on the muon beam characteristics in only a few minutes. We plan to use this to optimize those characteristics, measure them, and monitor them for long term stability in short dedicated periods interspersed with longer data sets without the TEC in place.

A further upgrade to the M13 beam line was completed during a beam shutdown in early 2004. A new vacuum isolation valve was installed near the F1 focus position, to take over part of the function of the previous combined beam blocker and vacuum gate valve, which proved unreliable in recent operation.

At the same time, a removable window valve was installed to solve a problem encountered in $\mathcal{TWIST}$ associated with the use of graphite production targets. When irradiated with the power of the proton beam, these targets emit radioactive isotopes into the beam line vacuum, which can migrate to decay within the beam tube that protrudes into the high solenoidal field. Much of the low energy β radiation is confined within the field and is sufficient to overwhelm and trip the normally very quiet chambers of the stack. A very thin (2.5 μm) polyester window was mounted on the removable paddle of a modified extra valve, also near F1. The membrane adds calculable depolarization, scattering, and energy loss of about 0.015 MeV/c (only 5% of the momentum acceptance width) to the surface muon beam. However, the gains from operation with a smaller, high luminosity graphite target make this a very profitable compromise.

From the outset, a gas degrader of length 20 cm has been in the muon path inside the solenoid, after a vacuum isolation window and immediately before the beam passes through the trigger scintillator and enters the detector stack. Since all of the materials are in the high field region, muon scattering does not cause appreciable depolarization. A variable mixture of He and CO_2 is adjusted so that the muon stopping position as measured by the detector planes is in the correct place. Because atmospheric density variations cause the position to move slightly, we are now providing automatic adjustment of the gas composition based on measurements of temperature and atmospheric pressure in order to compensate for their variations and to keep the muon stopping position precisely located. Its importance to the reduction of systematic uncertainties will be discussed later.

4 Data Analysis

4.1 Analysis Methodology

The challenge in the analysis is to select the e^+ emitted from μ^+ decays over the largest possible range of momentum and angle without introducing significant bias. This analysis is applied both to the data and the simulation and the results are compared to determine the decay spectrum. Biases in the analysis are then compensated to the extent with which the simulation accurately reproduces the data. The validation of the simulation then determines the associated systematic uncertainty.

Cuts based on the decay time do not produce angle/momentum biases. However cuts based on geometry clearly can produce such biases. The need for geometry based track selection is primarily driven by the presence of multiple tracks such as deltas or hard scatters. The identification and reconstruction of all tracks in this kind of event reduces sensitivity to the comparitive rates of such events in the data and the simulation. The $\mathcal{TWIST}$ detector has an intrinsic granularity determined by the plane and wire spacings. This results in some momentum-angle tracks being less well defined. Considerations such as these drive the analysis strategy.

Key elements of our analysis are:

- *Crosstalk removal:* This uses primarily the time width of the hit signals, but also checks for the existence of a generating signal. Only for the large ionization produced by muons is this effect significant.
- *Windowing:* Hits are separated into temporally isolated groupings using PC and DC information.
- *Classification:* Possible kinds of tracks within each window are identified by the topology of the hits. For the vast majority of events this topology is primarily temporal.
- *Pattern Recognition:* Tracks are identified through a fit to a helix of space points determined from clusters of wire hits within a window. More than one track candidate can be reported for each window. Delta rays tracks, which follow the magnetic field direction, are also indentified.
- *Wire center fits:* Helices are fit to the wire positions using the "narrow windows" technique [17]. Multiple scattering is included by allowing kinks at each sparse UV chamber pair position, constrained by the multiple scattering distributions [18]. The resulting fit has sufficient precision to resolve most left-right ambiguities.

- *Track fitting:* The particle trajectories are determined from fits to the hit times in the drift chambers incorporating space-time relations calculated from GARFIELD. The variable step size arc approximation is employed to integrate over the measured magnetic field map, and kinks are again introduced to account for multiple scattering.
- *Tree output:* Unbinned results of this analysis including track momenta and angle, classification and window information are output to ROOT trees (equivalent to hbook ntuples).
- *Energy calibration:* A fit to the upper edge of decay positron histograms in angle and energy derived from these trees is performed to correct the positron momenta for energy losses in the spectrometer, which have a $1/|\cos\theta|$ dependence on the decay angle. This fit also tests for a possible error in overall momentum scale.
- *Michel fits:* 2D histograms, binned using the energy calibration, are produced with appropriate fiducial cuts. These histograms are fit to analogous histograms from the simulation generated using hidden Michel parameters and their derivative distributions.

4.2 Progress in analysis software

4.2.1 Crosstalk

Crosstalk in the DCs is quite apparent for muon hits, but is much smaller for positrons. Crosstalk removal was investigated by studying the effect on efficiency of reconstruction of data. It was found that enabling crosstalk removal for data moves some events into the fiducial region, increasing the number by 0.4%, while moving 0.3% out of the region. These small numbers reflect the ability of our fitting procedure to ignore the spurious hits. Thus crosstalk removal is largely redundant for positrons, but produces a small increase in reconstruction accuracy. It is needed for μ^+ tracking. Simulation of crosstalk is not included in the Monte Carlo and thus crosstalk removal is turned off when analyzing Monte Carlo events.

4.2.2 Delta identification

The rate of the delta identification has been studied using simulated data, where we observed that the number of deltas identified varied linearly with the simulated production rate. Further, the number of deltas identified in the data is consistent with the number identified in the simulation. Delta identification is very important for validation of the simulation because we have to rely on the simulation to account for deltas produced below our detection threshold.

4.2.3 Pattern Recognition

New strategies have been used to reduce the incidence of reconstruction failures due to pattern recognition. Two independent routines have been written and compared both statistically and by visual event screening. The most effective technique involving the examination of all hit combinations has proven to be computationally practical, and is not the dominant factor in our CPU requirement. Reconstruction failures in simulation data below the 1% level (see Section 5.2, Fig. 15) . Perhaps 0.5% of the tracks are visually unrecognizable as helices, due to physics processes such as scattering, photo-production, delta production, *etc.* The 8 outer DC planes, which are densely spaced in z, proved to be very important for pattern recognition. The outer wires in these planes were not fully instrumented for the 2002 data, but this has now been remedied. Simulations show that this will result in improved reconstruction efficiency. Code has been written to allow use of both algorithms to maximize the reconstruction efficiency, but this was not utilized in the analysis of the 2002 data.

4.2.4 Helix fits

Multiple scattering (MS) is significant in the $\mathcal{TWIST}$ detector, despite its low mass, especially for high angle tracks where the effective thickness of chamber planes is greater. The scattering occurs mainly at the detector plane positions, and the focussing effects of the magnetic field make it non-trivial to visualize.

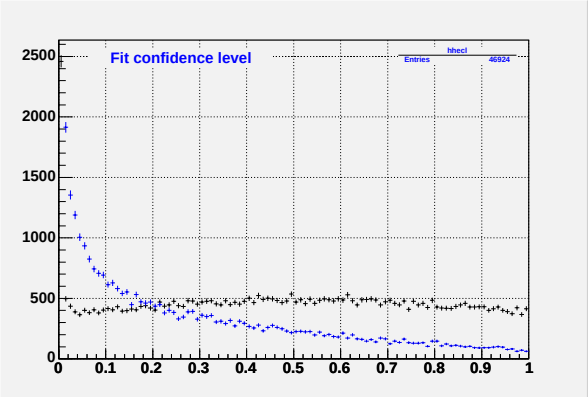

Figure 6: Confidence levels for wire-centre fits to helical tracks for data (left) and simulation (right). The flatter curves are for the fits including kinks.

Development of wire center fits with kinks and "narrow windows" [17] was completed. The method accounts for MS in the spectrometer and produces statistically reasonable confidence level distributions both in data and in simulations. Development then shifted to drift time fits to overcome limitations of wire center fits, such as excessive sensitivity to detector granularity, excessive biases at the edges of fiducial regions and lack of sensitivity to energy loss. As shown in Fig. 6, inclusion of MS using the kink method [18] greatly improved the confidence level distributions reported for wire centre fits. Since a uniform detector resolution function is used, the confidence level distributions for drift time fits cannot be expected to be flat. It is gratifying that the shapes are similar in data and MC. Figure 7 exhibits the development of the momentum and angular resolution obtained through these stages of analysis.

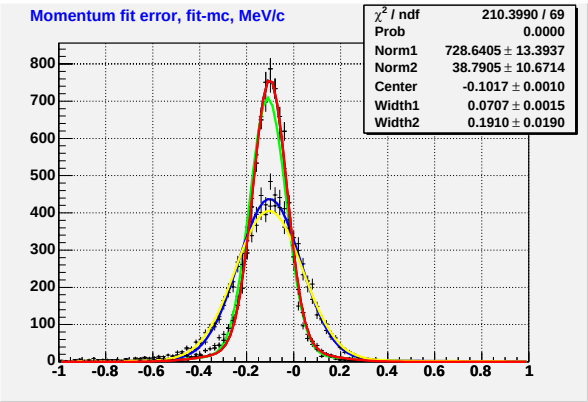

Figure 7: Momentum and angular resolution obtained from various tracking methods. Curves are : drift fit with kinks(red), drift fit no kinks (green), wire centre fit with kinks (blue), wire centre fit no kinks (yellow).

The effects of detector granularity can be understood by considering the track of a helix with pitch equal to twice the average plane pair spacing. The z-projection of such a track is a circle with the hits clustered at diametrically opposite points, so the circle radius is poorly determined. Such tracks challenge the pattern recognition and require the full accuracy of the helix fitter. Since the spacing of the outer 8 DC planes is much smaller than the inner ones, using these planes is very helpful for these difficult cases. It was decided for the 2003 data to instrument all the wires in these planes, at the cost of not recording some PC pulse height information, so they could be used in the tracking without bias.

There are several key software development projects for the coming year. The present fitter uses an averaged resolution function which ignores the variation of the resolution with distance from the wire. We plan to implement a maximum likelihood fitter with a more realistic resolution function

which matches measurement. This is also necessary for the development of a method of extracting the space-time relations in the DCs from the data. These improvements will address the systematic uncertainty that we have estimated by a long drift time cut. There is clear evidence in the 2002 data of changes correlated to the temperature and pressure in the chambers. These parameters are monitored online, and code will be written to adjust the STRs on a run-to-run basis, effectively a time interval of 15 minutes, to account for these variations. These changes are plane dependent, so the ability to use appropriate STRs needs to be coded. These corrections will reduce the systematic uncertainty arising from the precision of the STRs.

4.3 Calibrations

Calibration procedures have been refined during the past year. Our ability to calibrate is closely correlated to our ability to track. Calibration of the the relative TDC times can now be done both with straight and helical tracks. The fitting of 120 MeV/c pion tracks in zero magnetic field is used to determine translational and rotational alignments of chamber planes. Distortion in helical tracks from the expected shape is used to determine the orientation of the chambers to the magnetic field map.

Energy calibration is accomplished through fitting the kinematic end point of the Michel spectrum, which we parametrize over a narrow range of energy and angle by an analytic function. The angular dependence of this edge is given by $E_{meas} = (E_{kin} - \alpha/|\cos(\theta)|)(1+\beta)$ where α is the energy loss of a track at 0° and β is a possible scale factor for uncertainties in the magnetic field and detector dimensions. The global fit is done over bins of 0.2°. The region $p \geq 52$ MeV/c is selected over which the analytic approximation is adequate. Different values of α are used for upstream and downstream to allow for the muon stopping position. Figure 8 shows the quality of the fits, and the resulting angular dependence.

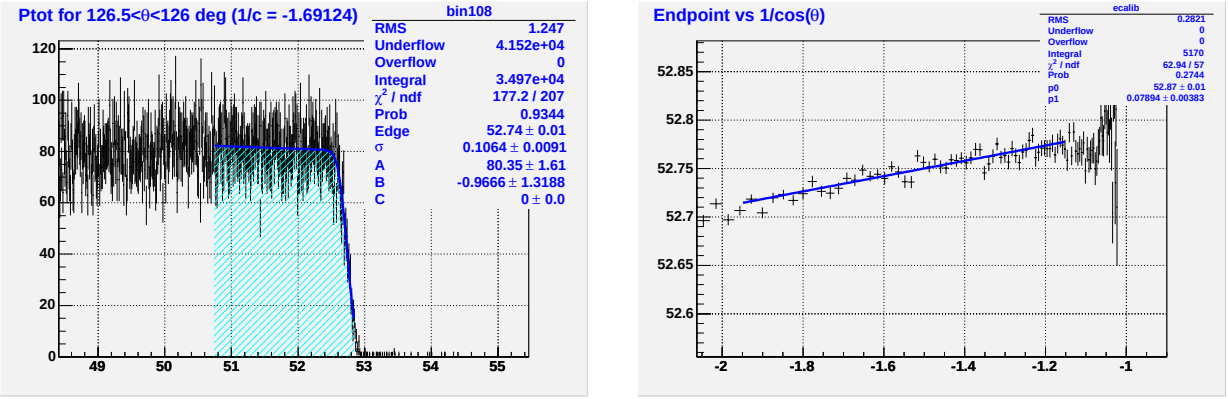

Figure 8: Left panel: Fit to the endpoint. Note that this figure is reproduced from an earlier version of the procedure, which used a different momentum range. Right panel: Angular dependence of the endpoints.

4.4 Extraction of decay parameters and blind analysis

To extract decay parameters from the experimental energy and angle decay positron spectrum, one needs to take into account detector response. In $\mathcal{TWIST}$, the detector response function is the probability density of reconstructing an event at $\{E, \cos(\theta)\}$ when "true" values are $\{E', \cos(\theta')\}$; *i.e.*, it is a scalar function of four variables. The convolution of the reconstructed spectrum is calculated directly by a Monte Carlo simulation program without the explicit knowledge of detector response. However a simulation requires not just the theoretical formula, but also a set of specific values of decay parameters to proceed, and the result is a convolution just for those values. To perform a fit for non-specific values of decay parameters, $\mathcal{TWIST}$ has developed a technique which uses an expansion of the convoluted

spectrum in deviations of the parameters from their MC values. The scheme can be visualized by

$$n_i(\alpha_{\rm Data}) = n_i(\alpha_{\rm MC}) + \frac{\partial n_i}{\partial \alpha}\,(\alpha_{\rm Data} - \alpha_{\rm MC}),$$

where $n_i(\alpha_{\rm Data})$ is the experimental spectrum, $n_i(\alpha_{\rm MC})$ is the simulated one, and $\Delta\alpha = \alpha_{\rm Data} - \alpha_{\rm MC}$ is the fit parameter. The $\partial n_i/\partial\alpha$ coefficient is calculated by Monte Carlo using analytical derivatives of the theoretical spectrum, where α stands for the decay parameters $\{\rho, \eta, \xi, \xi\delta\}$. Since the Michel form of the spectrum is linear in α, the first-order expansion is exact in this parametrization.

The simulated spectrum in the above description is in fact made up from *reconstructed* Monte Carlo events. $\mathcal{TWIST}$ uses the same reconstruction program for MC as for real data; thus any distortions introduced by the reconstruction software cancel exactly. The uncertainties that remain are how well the simulation recreates the real detector and the physics processes taking place. The detector uncertainty itself has already been minimized by design and construction, since the spectral distortion is small due to the low mass in the tracking region.

The fitting procedure described above allows for a straightforward "blinding" of the analysis: since the fit gives only the deviations from the MC values, it is enough to hide $\alpha_{\rm MC}$. The $\mathcal{TWIST}$ implementation of blind analysis uses asymmetric cryptography, and the only "secret" is the private key. Values of decay parameters for MC production are generated randomly, within given tolerances, and are used to produce a set of "decays" $\{E, \cos(\theta)\}$ which is stored on disk and can be fed to GEANT. The parameters are written down only in an encrypted form.

$\mathcal{TWIST}$ has implemented and tested all parts of the blind analysis software chain, from the "black box" spectrum generator to the fitter. For example, during analysis of the recently published results, we discovered and corrected an error in the treatment of radiative corrections in relation to the polarization terms. It was identified from an inconsistency in the value of δ derived from the cloud muon data set. Following the revelation of the hidden variables, analysis with the inconsistency corrected was checked by generating another simulation with the Michel parameters set to the experimental numbers, and it was verified that $\Delta\alpha$ were compatible with zero.

The system is also applied to the estimation of biases and systematic effects, where differences in decay parameters are determined from comparisons of data sets (real data or simulation) obtained under differing controlled conditions. This procedure has been used for the current publications.

4.5 Simulation Code

The current simulation code has been developed using GEANT 3.21. This simulation has an accurate description of the materials in and near the tracking region of the detector. Recent improvements include the incorporation of a realistic distribution of charge clusters produced by ionization in the chambers, leading to reasonable simulation of the observed spatial resolution. Detector translational and rotational (mis)alignments have been included in the simulation.

The phase space of the M13 beams used in 2002 were characterized this year using the same apparatus employed to establish the improved M13 tune. A significant improvement is the more direct measurement of the beam phase space using data taken with the time expansion chamber (TEC). Both the 2002 and 2003 beam descriptions are used as input to GEANT. The TEC geometry and digitization has been added to the simulation to validate the beam description. Space-time relations (STRs) for our chambers have been calculated using GARFIELD. The capability of using asymmetric STRs to model pressure-dependent bulges in the foils has been recently added. Additional modifications will be required to model plane-dependent asymmetries.

We have made careful studies of the GEANT3 navigator to validate its accuracy for tracking through volumes with different length scales, and have tuned the step sizes accordingly. The sensitivity of our results to the photon and positron energy thresholds has been found to be negligible. Simulation of chamber inefficiencies has been implemented, including random inefficiencies, inefficiencies in the cell corners, and those induced by highly ionizing muon hits.

Additionally we have carried out a series of comparisons between the GEANT3 and GEANT4 packages to explore differences which might affect our results. Development of a GEANT4 version of our simulation is in progress, and may be required to enable modeling of the positron interactions to the level needed for higher precision.

4.6 Computation Logistics

Much of the development and testing of our analysis software has been accomplished using our local cluster of some 30 computers, about half of which are desktop workstations. In November 2003 we became beta-testers of the WestGrid cluster at UBC, which increased our analysis capacity ten-fold. Although the initial implementation of the cluster experienced a period of some difficulties, we received excellent support from the WestGrid staff, and the bulk of the analyses for our recent publications was performed on the WestGrid cluster. As beta testers we often could run on more than 50% of the 1000 CPUs. The submission scripts that had been developed for the local cluster needed significant revision because of the configuration of WestGrid disk storage, and also because the database that we used was unable to handle the increased load. Instabilities in the storage and queuing systems during the beta period added additional complications. Development of scripts to organise the submission and storage of the data and simulations has required significant resources. We expect to continue using WestGrid as normal users under a share system. The local cluster machines are still used extensively for processing of ROOT trees, code development and testing, calibrations, and specialized analyses.

5 Status and Recent Developments

In the past two years, many milestones have been achieved. The major one is the first publication of $\mathcal{TWIST}$ physics results [3, 4], which will be summarized in the following sections. But for that to happen, several other tasks had to be accomplished. In 2003, many aspects of the analysis were improved (Section 4), including the addition of track kinks, drift time fits, and simulation as well as tracking with an accurate magnetic field map. All of these were crucial. To take advantage of that progress and the substantial first data sample obtained in late 2002, we needed powerful computing resources; we finally accessed these through WestGrid in the beginning of 2004, and since then, it has begun to provide us with reliable service. There have been developments summarized in previous sections in the muon beam line and its monitor (the TEC), the detector, the muon stopping target, and the analysis. In addition, there are many other improvements have occurred which are not described here in detail, such as to the slow monitoring and control systems.

Perhaps the greatest advance is the careful, realistic, and quantitative establishment of values or upper limits on systematic uncertainties. The ultimate strength of $\mathcal{TWIST}$ to put stringent limits on muon decay parameters will eventually be dominated by some of these uncertainties. We have learned much about which sources will likely be most important and which will not require much further study. We do not have to rely on simplistic models to defend our estimates, as we did in some cases before we had data, detailed and verified simulations, reliable analysis software, and the computing power to apply them to systematic estimations.

5.1 Determination of systematic uncertainties

The determination of systematic uncertainties was a major component of the data analysis leading to the first publications of results for ρ and δ. Due to space constraints, it is not possible to present a full and detailed account here. The following summary covers the method and examples of the techniques employed and includes the final results.

The process began with a list of candidate sources of systematic error. This list evolved over the course of several years and was based on a variety of calculations and estimates. These numbers were based largely on analytical estimates or toy Monte Carlo simulations. For ρ and δ the largest contributions were anticipated to come from the energy calibration, alignment, and the response function.

The list of candidate sources of systematic error helped to guide the run plan for the 2002 data, which included a variety of data sets taken under different conditions:

1. Solenoid fields – 1.96 and 2.04 T.
2. Trigger rates – 1.18 and 4.7 KHz.
3. Muon stopping position – slightly upstream and slightly downstream.
4. Drift chamber HV – 1850 V and 1950 V.

5. Proportional chamber HV – 1900 V.
6. External material – plates of 0.25" Al, 0.25" plastic, 0.5" plastic placed at the downstream exit of the detector stack.
7. Beam – cloud muons.
8. Nominal sets – two under standard conditions, separated by several weeks.

In addition to the nominal data sets and some to check the consistency of the measurements, others were taken with a specific parameter exaggerated to enhance the effect on the Michel parameters. The resulting change in Michel parameters is an estimate of the *sensitivity* to the difference in spectrum shape.

Only a few of the systematics parameters could be studied directly from data. Most of the remaining systematic sensitivities were determined by fitting a data or MC sample analyzed with a systematic parameter offset from its nominal value to the same sample analyzed with this parameter at its nominal value. Usually this could be studied using a correlated analysis, which resulted in an improved precision for the comparison. In constructing the list of studies, every effort was made to keep the terms as orthogonal as possible.

In many cases the resulting sensitivities were within the statistical limits of these tests. This is illustrated in Fig. 9, which shows the sensitivities for most terms for both ρ and δ using the results from the final analysis for δ. It is clear that often the statistical error on the sensitivity is not sufficiently small to yield a significant measure of the sensitivity. However, as will be seen later, the limits on the systematic uncertainties are still acceptable and will be improved in the future.

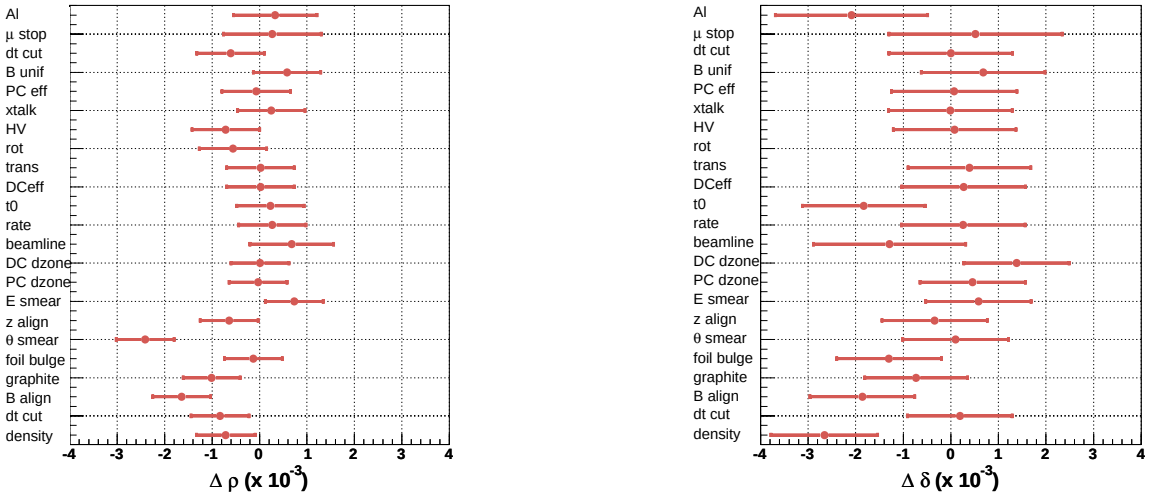

Figure 9: Sensitivities for systematics of ρ and δ. The values are divided by scale factors to determine systematic uncertainties.

The systematic uncertainty is determined by dividing the sensitivity for each parameter by a scale factor that is the ratio of the exaggeration divided by an estimate of the range of that parameter in the data. Terms that were expected to be the same for all data sets were tabulated separately from those that could change from one data set to another. Examples of set-independent terms were those for alignment and those related to the physics of positron interactions. Set-dependent terms included those for the foil bulge and for magnetic field distortion.

The scale factors are summarized in Table 2 and details for the alignment are presented as an example of set-independent terms. The scale factor for translational alignment is 28 because the sensitivity study was done with an exaggerated random misalignment with an rms variation of $\sigma = 140$ μm, while the accuracy of the plane to plane alignment was 5 μm. Similarly, for rotations of the planes, the random misalignment was 0.39°, while the uncertainty was 0.004°. Along the beam axis the chamber

positions were known to 30 μm and the alignment between the axis of the detector and the magnetic field was known to 1.2 mrad. In a few cases the scale factors are different for ρ and δ. The detector alignment to the B field is one such case where the estimated uncertainty was increased after the ρ analysis was completed. Another case was the effect of the dead zone, where further analysis led to an decrease in the systematic uncertainty.

One of the set-dependent terms was due to uncertainties in the magnetic field map. The scale factor for the 2 T field data was 10, but larger uncertainties for the 1.96 and 2.04 T data led to smaller scale factors of -4 and 2.

A source of systematic uncertainty that turned out to be significant was due to changes in the foil positions resulting from changes in differential pressure between the chamber gas and the He/N_2 mixture between chambers. The resulting change in chamber half-gap changed the space-time relation (STR) for the drift chambers. Other factors that were important for the STRs were the chamber high voltage and the gas density, which was sensitive to changes in temperature or atmospheric pressure. The plots in Fig. 10 provide information about the relative contributions of different terms. Each data set is a string of points in the top and middle graphs. The (reduced) χ^2 is for the helix fit; larger values correspond to poorer fits if the STR values are not optimum. The upper-left plot shows that within a data set the χ^2 is correlated with density and the upper-right plot shows the χ^2 values after correction for density. The latter values are quite constant within a data set, but the vertical separation of sets indicates another important variable is changing. The middle plot shows the behavior versus time. There is excellent correlation with the bottom plot, which shows errors in the differential pressure measurements due to gas density changes in the pressure sense lines and are an indirect measure of the foil position. The graphs show that the foil bulge grew with time before it was reset. One set that falls off the general trend was taken with a different HV, showing the importance of yet another term.

The results for most of the systematic uncertainties are given in Table 2 and shown graphically in Fig. 11 for δ (the plot for ρ is similar). Two of the systematic uncertainties were determined using a different technique than for those discussed above. The uncertainty for the energy calibration end-point fits was determined from the statistical error on the energy calibration parameters from fits to each data set. The analysis for the uncertainty due to the GEANT simulation of hard-interactions was somewhat complicated and will be described in detail.

There is a single line for hard interactions, but it includes both intermediate and hard interactions, with a somewhat arbitrary division between the two. Intermediate interactions are those – beyond the simple shift due to energy loss – that lead to a change in the positron momentum of less than 1 MeV from the time of the decay until it is last seen in the drift chambers. Most of this probably comes from the long low-energy (Landau) tail on the energy loss distribution. This is measured by examining a plot of the (reconstructed/thrown) MC momentum spectrum for those positrons that lose less than 1 MeV. The net change in the yield over the range from 30-50 MeV is $\sim 0.3\%$ for the angular range $0.7 < |\cos\theta| < 0.84$ and 0.17% for the angular range $0.5 < |\cos\theta| < 0.7$.

Hard interactions are those that lead to a change in the positron momentum of greater than 1 MeV from the time of the decay until it is last seen in the drift chambers. The relevant plot shows that the corresponding (reconstructed/thrown) momentum spectrum has a net change in the yield of $\sim 0.37\%$ and 0.47% over the range from 30-50 MeV for the same angular ranges.

To estimate the corresponding uncertainty in ρ, we show by comparisons with validation data that GEANT handles the soft physics well at the 5% level and the hard physics well at the 14% level, then add the two contributions linearly. The uncertainty is dominated by the limited statistics of our experimental validation of GEANT, which we can easily improve in the future. Finally, we multiply the result by 0.68 for ρ, since $\Delta\rho = -0.001$ leads to an increase in the relative yield of +0.00147 over the range from 30-50 MeV. Overall, we get a systematic uncertainty in ρ of 0.45×10^{-3} and 0.51×10^{-3} using this procedure for the two angular ranges. We take 0.45×10^{-3} from the larger $|\cos\theta|$ range, which has the bigger momentum reach so it plays a bigger role. This also provides some recognition of the double counting issue due to uncertainty in the target thickness.

In summary, for the current analysis the largest uncertainties for ρ arise from the time variations of the cathode foils and the density of the DME gas, which change the drift velocities and influence the DC efficiencies far from the sense wires. These parameters were monitored throughout the data accumulation periods and an average value was used in the analysis. Other important effects arise from the uncertainty in the thickness of the graphite layers on the Mylar target and from uncertainties in the GEANT treatment of positron interactions that lead to spectrum distortions. The target thickness issue was studied by varying the thickness of the graphite coating in MC. Upper limits for the positron

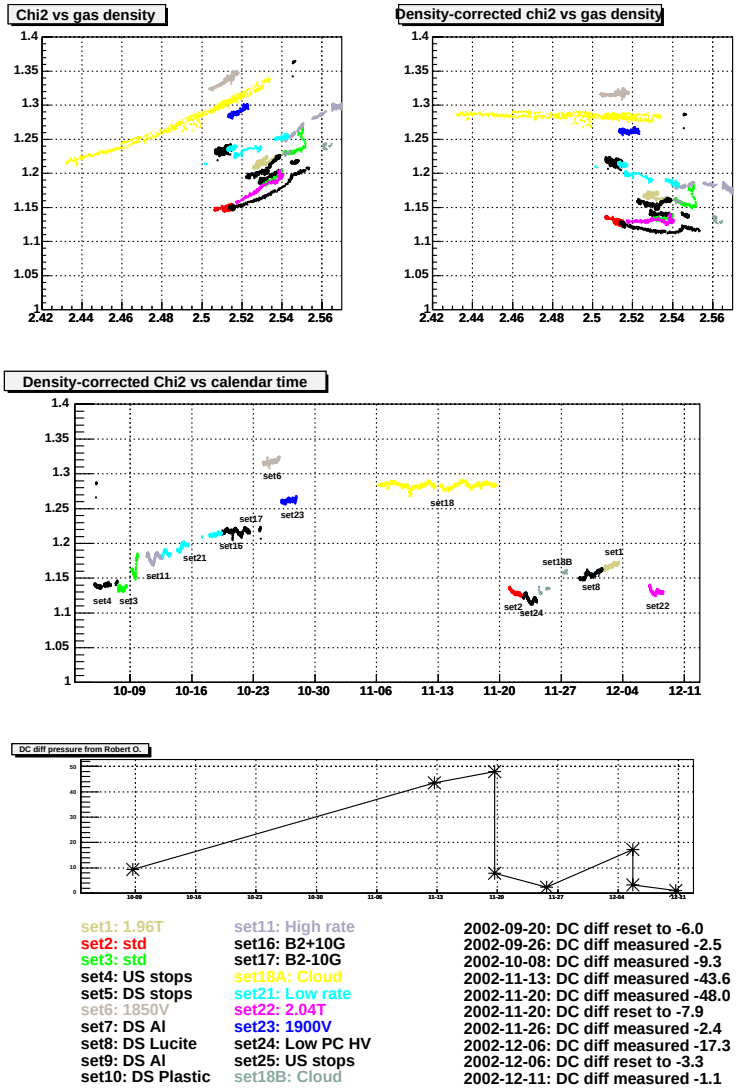

Figure 10: χ^2 versus density or time for runs in most data sets. See text for more information.

interactions uncertainties were derived from studies of the data for muons stopped far upstream (Section 5.2) and from MC histograms that demonstrated the distortion of the momentum spectrum due to hard interactions. The largest uncertainties for δ are for the detector alignment, for the simulation of positron interactions, and for the chamber response, in particular the time dependent effects due to gas density changes and to the variability of the cathode foil positions.

5.2 First $\mathcal{TWIST}$ results

The calculation of systematic uncertainties as described in the previous section has allowed us to submit for publication the first physics results from $\mathcal{TWIST}$, consisting of simultaneous measurements of the muon decay parameters ρ and δ. These are also the first measurements in 35 years to improve the independent measurements of ρ, and the first in 15 years to improve δ.

The final results are

$$\rho = 0.75080 \pm 0.00044(\text{stat}) \pm 0.00093(\text{syst}) \pm 0.00023(\eta) \quad (14)$$

$$\delta = 0.74964 \pm 0.00066(\text{stat}) \pm 0.00112(\text{syst}) \quad (15)$$

	ρ	scale	$R'\sigma$	ave	δ	scale	$R'\sigma$	ave
Positron interactions			**0.46**				**0.55**	
Energy smearing	-0.02	4	0.00		0.58	4	0.15	
Multiple scattering	-2.26	20	-0.11		0.1	20	0.01	
Hard interactions			0.45				0.53	
Material outside the detector	0.53	60	0.01		-2.09	60	-0.03	
Material in detector (graphite)	-0.98	2	**-0.49**		-0.73	2	**-0.37**	
Spectrometer alignment			**0.22**				**0.61**	
Translations	0.07	28	0.00		0.39	28	0.01	
Rotations	-0.56	10	-0.06		-4.33	78	-0.06	
z	0.44	10	0.04		-1.07	10	-0.11	
B field to axis	-1.49	7.2	-0.21		-1.86	3.1	-0.60	
Chamber response (ave)				**0.51**				**0.56**
DC efficiency	0.64	50	0.01		0.27	50	0.01	
PC efficiency	-0.108	50	-0.00		0.07	50	0.00	
Dead zone	0.54	4	0.14		0.45,1.38	6,15	0.12	
Long drift time clip	0.48	1	0.48		0.15	4	0.04	
HV variations (DC,PC)	-0.70	20	-0.04		0.08	20	0.00	
Temperature and pressure (ave)	-0.51			-0.01	-2.66			-0.13
Foil bulges (ave)	-0.053			-0.01	-1.3			-0.35
Crosstalk	0.25	10	0.02		0.00	10	0.00	
t0 variations	0.23	10	0.02		-1.83	10	-0.18	
Momentum calibration (ave)				**0.17**				**0.29**
End point fits			0.15				0.22	
Magnetic field reproduction (ave)	0.58			-0.08	0.68			-0.10
Muon beam stability				**0.04**				**0.10**
Stopping location	0.17	6	0.03		0.52	6	0.09	
Beam intensity	0.16	6	0.03		0.26	6	0.04	
Channel magnets	0.84	50	0.02		-1.29	50	-0.03	

Table 2: Summary of systematic uncertainties for ρ and δ in units of 10^{-3}. The columns show systematic sensitivities, scale factors, and scaled variations ($R'\sigma$) as individual contributions to different categories of total systematic uncertainties, along with averages (ave) for data sets where appropriate.

where the last quoted uncertainty for ρ is due to the uncertainty in the assumed value for $\eta = -0.007 \pm 0.013$, which was held fixed in the analysis. Unlike any previous muon decay parameter measurements, the analysis was done with the true decay parameters hidden (see Section 4) in a so-called "blind analysis", and systematic uncertainties were determined prior to revealing the hidden values. While these are only the first results from $\mathcal{TWIST}$ they represent advances in experimental precisions compared with previous results (see Section 2) by factors of 2.5 for ρ and 2.9 for δ.

The data consisted of about 6×10^9 muon decay events from Fall 2002, divided up into data sets of typically 3×10^8 events. Five sets were used to extract ρ: two sets at nominal conditions, two at different solenoid fields (1.96 and 2.04 T), and one using cloud muons which have lower polarization ($\sim$30%) and opposite polarization direction. The same data sets, with the exception of the low polarization cloud muon set, were used to find δ. The remainder of the data sets were used for the purpose of systematic estimates.

It is essential that we understand the response function of the $\mathcal{TWIST}$ detector, because the analysis method relies on comparison with the simulation, which in turn must accurately represent the response. There are few possibilities for a direct measurement of the $\mathcal{TWIST}$ response to monoenergetic and/or monodirectional positrons. Radioactive sources are too low in energy, while the two-body decay $\pi \to e\nu$ is above our momentum range, has low branching ratio, and has characteristics making it difficult to produce and separate with high statistics in $\mathcal{TWIST}$. We have nevertheless been able to show from some tens of events that it does agree with what we predict.

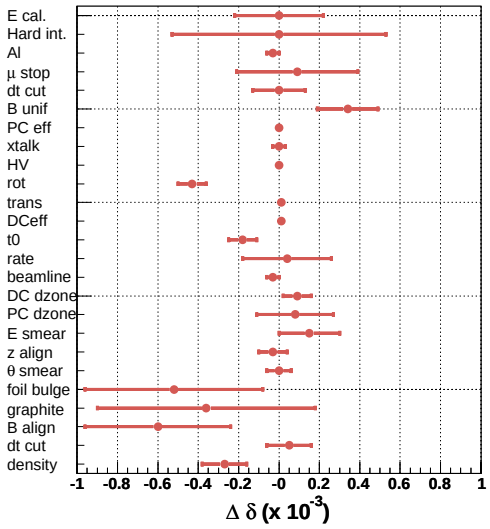

Figure 11: Systematic uncertainties for δ in units of 10^{-3}.

There is, however, a method to test the response function predicted by the simulation in a reasonably straightforward way. Since the detector stack is naturally split into two independent positron spectrometers, real decay positrons can be measured twice, once in each half of the stack, by arranging for muons to stop near either the entrance or exit of the spectrometer rather than in the middle. Measurement of the difference of momentum and angle between the two halves, for beam data and simulated data, will show any weakness of the simulation and test not only how the response function is reproduced but also how well the simulation handles energy loss and multiple scattering, including hard scattering tails, of positrons in our fiducial range. The differences in measurements of two segments of a decay positron track are shown in Fig. 12. Momentum or angle differences can be displayed either as a function of momentum or angle; Fig. 13 shows the momentum difference plotted with respect to momentum.

Figure 14 shows a comparison of momentum spectra near the kinematic end point for surface and cloud muon data sets, each one for two restricted angular ranges corresponding to upstream ($\cos\theta < 0$) and downstream ($\cos\theta > 0$) decays. In the normalized plots, the difference in polarization direction and magnitude is clear. The simulation reproduces the shape of the end point distributions. It is the comparison of these regions, for many different angles, that is used in the energy calibration procedure (Fig. 8).

The ρ parameter determines the momentum dependence of the positron in positive muon decay. Figure 15 [3] shows the muon decay spectrum momentum dependence as measured for one of our data sets, and also indicates the momentum within this angular range which falls within our defined fiducial region where $p < 50$ MeV/c, $|p_z| > 13.7$ MeV/c, $p_T < 38.5$ MeV/c, and $0.50 < |\cos\theta| < 0.84$. The normalized residuals of the fit of the simulation spectrum, including derivative components according to the fitting strategy described in Section 4, are also shown for two angle ranges. The other graphs depict how the response function of the detector moves events in this momentum range.

The δ parameter determines the momentum dependence of the asymmetry of the positron in polarized positive muon decay. As shown in Fig. 16 [4], the $\mathcal{TWIST}$ spectrometer measures the linear dependence of the yield on $\cos\theta$, except for ranges near zero and ± 1 where decay track parameters cannot be well determined. Figure 17 summarizes the asymmetries from a larger momentum range. The asymmetry changes sign for the lowest momenta. Again, a high quality fit to the simulation is obtained.

From the results for ρ and δ we are able to set constraints on certain parameters. The measured ρ constrains the mixing angle ζ (Eq. 12) in the left-right-symmetric model to be less than 0.030 (90% c.l.). Using a previous limit for $P_\mu \xi\delta/\rho$ [14, 15] and the fact that $Q_R^\mu \geq 0$, Eq. 6 leads to the limits

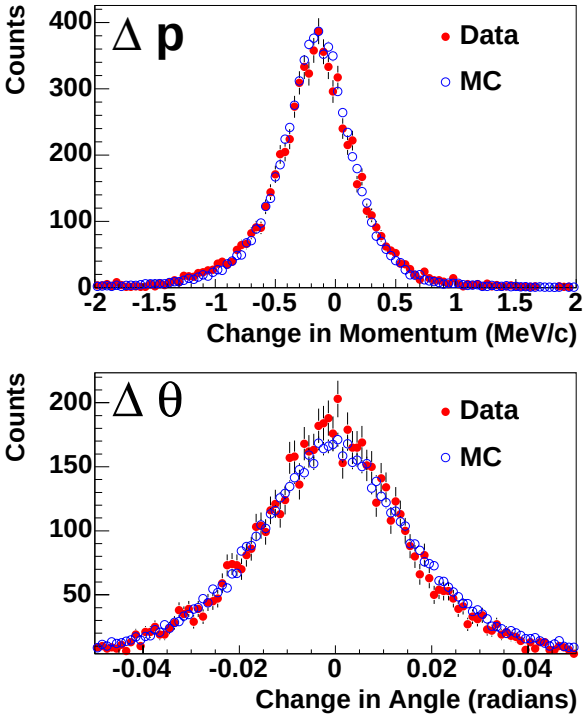

Figure 12: The difference between downstream and upstream tracks, for both data and MC, resulting in: Top, the positron momentum change in the central stopping target, Bottom, $\Delta\theta$ for a positron that passed through the central stopping target. The MC results were normalized to those of the data for the purposes of this figure.

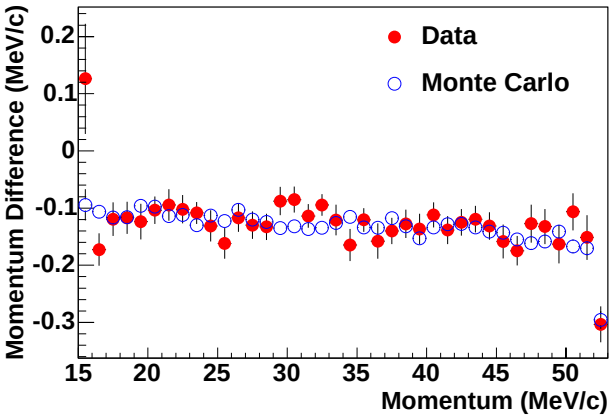

Figure 13: Average energy loss of decay positrons through the target and detector materials as a function of momentum for data (closed circles) and Monte Carlo (open circles), measured as described in the text.

(90% c.l.) $0.9960 < P_\mu\xi \leq \xi < 1.0040$, which are more restrictive than current direct measurements of $\mathcal{P}_\mu\xi$. The lower limit increases the lower limit on the mass of W_R slightly (via Eq. 12).

Estimating systematic errors on the direct measurement of $\mathcal{P}_\mu\xi$ from 2002 data is questionable because of the observed depolarization in the graphite-coated Mylar target. We observed systematic variations in the fitted value of ξ between different sets. If depolarization is different in the graphite coating and the Mylar, differences in the mean stopping positions within this target would lead to such variations. These differences came about due to several factors, such as ambient gas density (temperature and pressure; see discussion of Fig. 10) changes and also the foil bulging problem discussed in Section 5.1. Changes due to both of these are being controlled more closely, and the target is now high purity aluminum. We know from 2003 data that in the high purity aluminum target the estimated $\mathcal{P}_\mu\xi(0)$ at time zero with statistical error only is about 99.7±0.2%, based on a simple model of polarization in terms of integrated angle distributions, *i.e.*, not a full 2-d fit to simulated data. For the beam tune used in 2003 this measurement is consistent with our estimates of depolarization of muons in the solenoidal magnet fringe field. A comparison is shown in Fig. 18. While this simple estimate shows no evidence of initial depolarization (*i.e.*, extrapolated to time zero), there is certainly an indication of time-dependent depolarization, which is much less problematic as it can be included in the simulation in the equivalent of a systematic correction. However, this should not be necessary, since the observed time dependence is likely due not to muons stopping in the Al target but in the materials of the adjacent detector PC6. They also satisfy our usual PC6 $\cdot\ \overline{\text{PC7}}$ analysis requirement. By dedicated running with the muon stop position adjusted slightly upstream of the target, we can measure depolarization and its time dependence for stops in PC5 only by using PC5 $\cdot\ \overline{\text{PC6}}$ as an analysis requirement. The depolarization

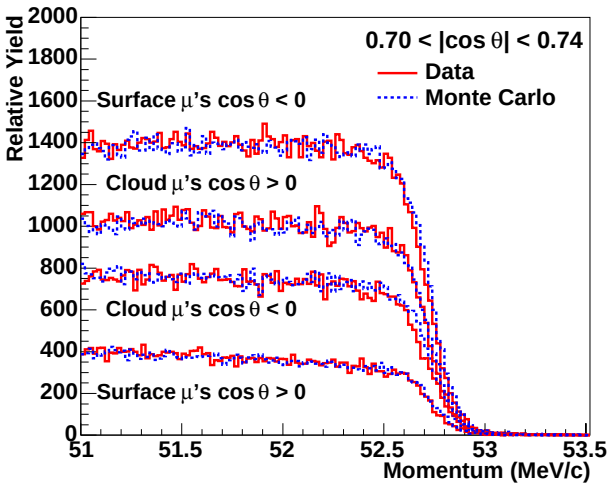

Figure 14: (above) Measured positron momentum spectra (solid lines) near the end point are compared to Monte Carlo simulations (dotted lines). The curves show surface muon set B for $-0.74 < \cos\theta < -0.70$, cloud muons for $+0.70 < \cos\theta < +0.74$, cloud muons for $-0.74 < \cos\theta < -0.70$, and surface muon set B for $+0.70 < \cos\theta < +0.74$.

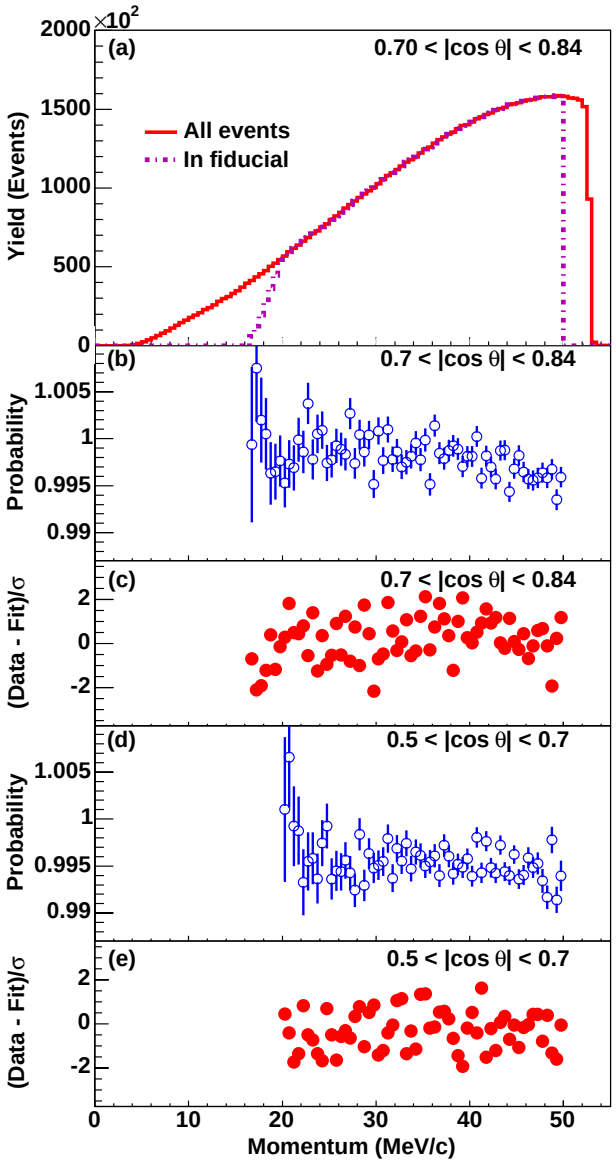

Figure 15: (right) Panel (a) shows the muon decay spectrum (solid curve) from surface muon set B as a function of momentum, for events with $0.70 < |\cos\theta| < 0.84$, as well as the events within this angular region that pass the fiducial constraints (dot-dashed curve). Panels (b) and (d) show the probability for reconstructing muon decays for two angular ranges, as calculated by the Monte Carlo. Panels (c) and (e) show the residuals for the same angular ranges from the fit of set B to the Monte Carlo 'standard' spectrum plus derivatives.

and its time dependence can be explicitly accounted for in our simulation.

In 2004 and 2005 we will obtain data for the remaining systematic error estimates needed for $\mathcal{P}_\mu\xi$. A data set will be included with a collimated beam to reduce the influence of fringe field depolarization.

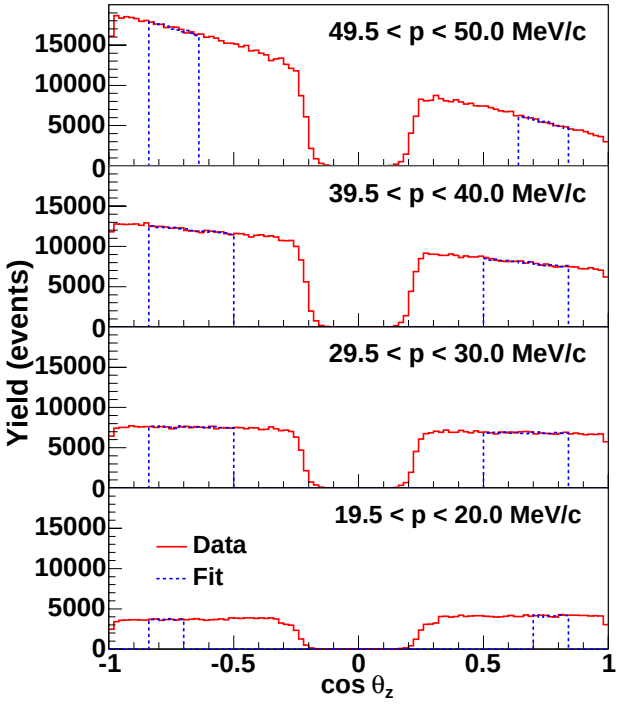

Figure 16: Decay positron angular distributions from set B (solid curves) and the corresponding best fit distributions within the fiducial region (dashed curves) for selected momentum bins.

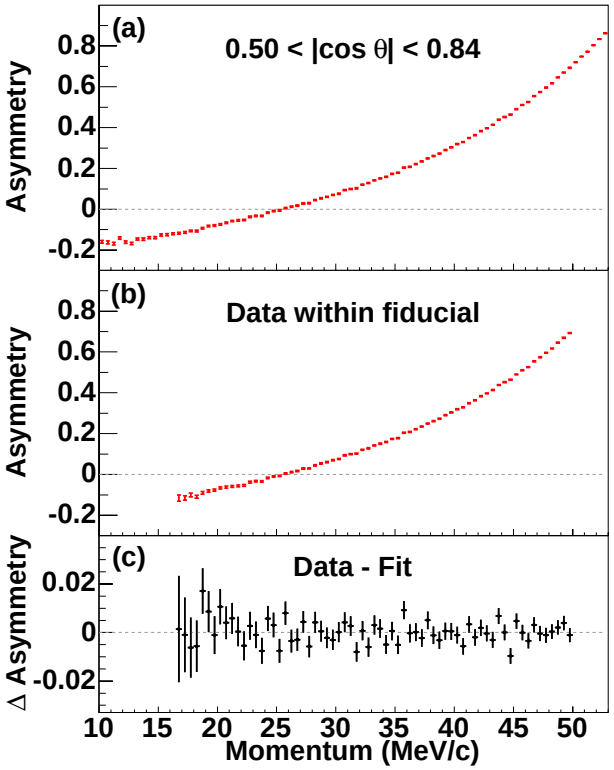

Figure 17: (a) The observed muon decay asymmetry from set B for all events within $0.50 < |\cos\theta| < 0.84$. (b) The same quantity for those events that fall within the fiducial region. (c) The difference between the data in panel (b) and the best fit MC spectrum.

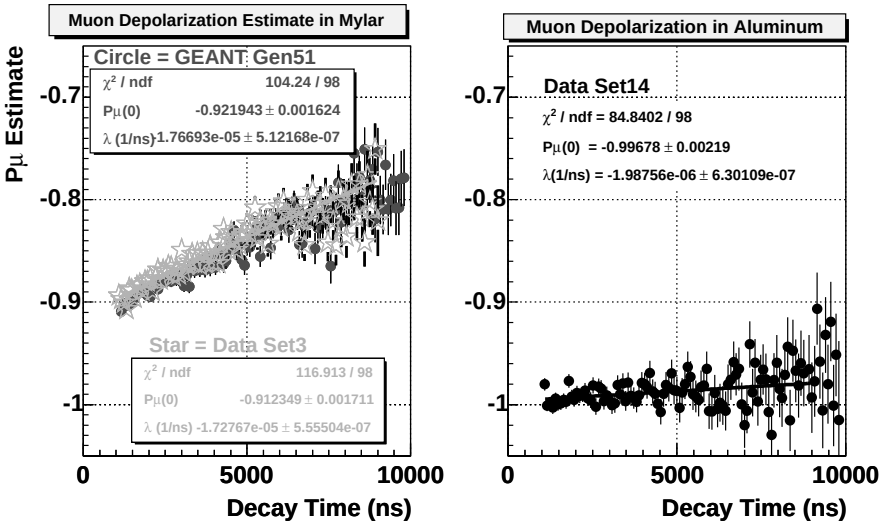

Figure 18: Time dependence of asymmetry for graphite-coated Mylar (left) and high purity aluminum (right) targets.

6 Improving Precision for $\mathcal{TWIST}$

The experience gained in the first measurements of the muon decay parameters allows us to anticipate with much more confidence the tasks which are most important to attaining $\mathcal{TWIST}$'s final goals. At least for ρ and δ, we know which systematics can be expected to dominate, and we know how all of them can be reduced. Obtaining the final reductions in systematic uncertainties will be extremely challenging, of course, and we still need to gain the essential experience for $\mathcal{P}_\mu\xi$ by going through that analysis in a coherent way. We have identified necessary improvements to the detector and beam line systems, and have implemented or planned their realizations; many of these issues have already been discussed. The constituents of the analysis and its framework have advanced considerably. We know the main remaining weaknesses and how gains can be made.

6.1 Statistical requirements

The projections for statistical errors and systematic uncertainty requirements can be scaled from the actual experience from the 2002 data. These data yielded precisions for the Michel parameters as given in the second column of Table 3 for a data set, which is loosely defined as 2 days of data or $\sim 3\times10^8$ events. The next three columns give the statistical, systematic and total errors for ρ and δ from the just-completed analyses, which were based on 5 sets for ρ and 4 sets for δ. The statistical precision for ρ is quoted before inflation by the S factor, which represents systematic uncertainties which are otherwise unaccounted for [6]. The time available for 2004 data, as of the preparation of this proposal, is $\sim$30 days or 15 sets. Of these, approximately 7 are allocated for systematics studies and 8 for data. With the need to make several upgrades to $\mathcal{TWIST}$ work properly (*e.g.*, graphite target and TEC) it may be necessary for this running period to continue in April 2005. The statistical precision that can be expected from this amount of data in 2004-2005, without taking into account any improvements in the analysis or in MC statistics, is given in the sixth column labelled "2004-2005:8 sets". The stated goals of a factor of 2 improvement for ρ and δ and a precision of 10^{-3} for ξ result in the entries in the eighth column labelled "2004-2005:total". From the entries in these two columns the target values for systematic uncertainties can be deduced and are shown in the seventh column labelled "2004-2005:sys". Similarly, for the final goals of a factor of 10 improvement over current published values for ρ and δ and an improvement of 20 for ξ, the desired total errors are given in the last column labelled "final:total". Assuming equal contributions from statistics and systematics for ξ, the required precisions for statistics and systematics are given in ninth and tenth columns labelled "final:stat" and "final:sys". A statistical precision for ξ of 0.30×10^{-3} will take about 3 months of data (without improvements) and the corresponding precision for ρ and δ from the same quantity of data are also listed in the column labelled "final:stat". The required systematic uncertainties for δ and ξ are then deduced in the corresponding lines in the column labelled "final:sys". The time required for running to address systematics will be based on what is learned from the 2004-2005 runs, but will probably be at least as much as is required for statistics.

	2002	2002			2004-2005			final		
parameter	stat/set	stat	sys	total	8 sets	sys	total	stat	sys	total
ρ	0.7	0.32	0.96	1.07	0.25	0.37	0.5	0.10	0.24	0.26
δ	1.3	0.66	1.12	1.25	0.53	0.28	0.6	0.22	0.32	0.39
$\mathcal{P}_\mu\xi$	1.9				0.72	0.69	1.0	0.30	0.30	0.43

Table 3: Michel parameter uncertainties in units of 10^{-3}.

The predictions for statistical requirements are conservative because expected improvements in the reconstruction codes will permit the fiducial region to be increased. Also, polarization for the 2002 data was slightly reduced, which lowered the sensitivity to the Michel parameters for δ. Most importantly, for the 2002 data the MC statistics were equal to the data statistics resulting in a 41% inflation of the error. With MC statistics of 3 times that for the data, the errors are inflated by only 15%, and with 4 times, the inflation is 12%. Thus a reasonable specification for the MC to match the 2004 data is (10 sets)$\times$(3 times)$\times 2\times10^8$ events per set, or 6×10^9 MC events.

6.2 Status of systematics for 2004 running

The goal of the run in progress (Fall 2004) is to yield a measurement of $\mathcal{P}_\mu\xi$ at the level of 10^{-3} and to improve the precision on ρ and δ by a factor of 2. The experience gained from 2002 data helps to give us reasonable confidence that these goals can be met, although learning to make optimal use of the TEC and a graphite target may result in some engineering aspects to this period, and we may continue in April 2005.

Table 4 shows the systematic uncertainties for ρ, δ, and ξ after application of scale factors and renormalization of the errors using the analysis code adopted for the δ result. The lines for hard scattering and for energy calibration do not have central values since these were obtained using alternate techniques (see Section 5.1). The last 4 lines are for ξ-specific terms and were estimated separately.

							goals		
	ρ	$\Delta\rho$	δ	$\Delta\delta$	ξ	$\Delta\xi$	ρ	δ	ξ
density	-0.07	0.06	-0.27	0.11	0.24	0.14	<0.05	<0.05	∼0.05
drift time cut (MC)	-0.21	0.06	0.05	0.11	-0.03	0.13	∼0.05	∼0.05	∼0.05
field-detector alignment	-0.53	0.2	-0.6	0.36	0.39	0.46	<0.05	<0.05	<0.05
detector material (graphite)	-0.51	0.3	-0.36	0.54	0.48	0.69	<0.05	<0.05	<0.05
foil bulge	-0.05	0.24	-0.52	0.44	0.89	0.56	∼0.05	∼0.05	∼0.10
θ smear	-0.12	0.03	0	0.06	-0.16	0.07	∼0.05	∼0.05	∼0.05
z align	-0.06	0.04	-0.03	0.07	0.02	0.09	∼0.06	∼0.07	∼0.09
energy smear	0.18	0.08	0.15	0.15	-0.07	0.19	∼0.05	∼0.05	∼0.05
dead zone (PC)	0	0.1	0.08	0.19	-0.32	0.24	<0.05	<0.05	∼0.05
dead zone (DC)	0	0.04	0.09	0.07	-0.22	0.09	<0.05	<0.05	∼0.05
beam line	0.01	0.02	-0.03	0.03	-0.18	0.04	∼0.02	∼0.03	∼0.18
beam rate	0.04	0.12	0.04	0.22	-0.5	0.28	<0.05	<0.05	∼0.05
t0	0.02	0.04	-0.18	0.07	0.49	0.09	<0.05	<0.05	∼0.05
DC efficiency	0	0.01	0.01	0.01	0	0.02	<0.05	<0.05	<0.05
translational alignment	0	0.01	0.01	0.02	0	0.02	<0.05	<0.05	<0.05
rotational alignment	-0.01	0.00	-0.06	0.01	0.11	0.01	<0.05	<0.05	<0.05
HV stability	-0.04	0.01	0	0.02	-0.02	0.03	∼0.04	∼0.02	∼0.03
crosstalk	0.02	0.02	0	0.03	0	0.04	∼0.02	∼0.03	∼0.04
PC efficiency	0	0	0	0.01	-0.01	0.01	<0.05	<0.05	<0.05
field uniformity	0.29	0.08	0.34	0.15	-0.47	0.19	∼0.12	∼0.14	∼0.20
drift time cut (data)	-0.15	0.07	0	0.13	-0.17	0.17	∼0.05	∼0.05	∼0.05
μ stop	0.05	0.17	0.09	0.3	4.55	0.4	∼0.05	∼0.10	∼0.10
Al	0.01	0.01	-0.03	0.03	0.02	0.03	<0.05	∼0.03	∼0.03
hard interactions		0.45		0.53		0.60	∼0.15	∼0.18	0.20
energy calibration		0.15		0.22		0.27	∼0.05	∼0.07	∼0.09
depolarization in target					-0.04	0.02			∼0.04
cloud muon contamination						0.12			∼0.12
fringe field						0.30			∼0.30
proton beam					-0.30	0.07			∼0.30
						total:	0.25	0.30	0.61

Table 4: Systematic uncertainties with errors for ρ, δ, and ξ from the current analysis, and goals for the 2004-2005 run. The units are 10^{-3}.

The target total systematic error for ρ is 0.37 (all quantities in this discussion are in units of 10^{-3}.) Of this, 0.23 is due to the uncertainty in η and cannot be reduced without a new measurement of η with improved precision. Also we assume the uncertainty in the theoretical radiative corrections of 0.20 will not be reduced soon. This leaves a target of 0.21 for the rest, which currently is 0.88 (without the S factor which scales systematic uncertainties to achieve a reduced χ^2 of one [6]).

By making realistic improvements it should be possible to reduce the systematics uncertainties to the values listed in the goals columns of Table 4. For example, the uncertainty due to the target

thickness will be reduced by an order of magnitude by virtue of the change to an Al target of known thickness. The drift-time cut uncertainty will be reduced significantly through direct extraction of drift time distributions from the data, rather than relying on GARFIELD calculations. Validating GEANT to 5% from 14% will reduce the uncertainty for hard interactions by a factor of three. Explicitly applying an alignment of the detector to the B field will reduce this term by an order of magnitude. An improved energy calibration algorithm will be required to reduce the uncertainty in the end-point fits by a factor of 3. Additional studies of the dead zone already indicate the uncertainty should be much smaller. Additional MC studies will be required to reduce the uncertainty due to multiple scattering and energy smearing by a factor of 2.

Some terms will be reduced by improving operating conditions during the 2004-2005 run. The differential pressure will be monitored more closely, which will help reduce the uncertainty due to the foil bulge. The uncertainty due to the muon stopping distribution will be reduced by active control of the gas degrader. The beam rate will be monitored more closely and large excursions can be excluded from the data analysis.

Other terms will be reduced by tracking changes during the analysis. For example, the t0 values will be adjusted more often, and the systematic uncertainty for density will be reduced by using time-dependent STR tables.

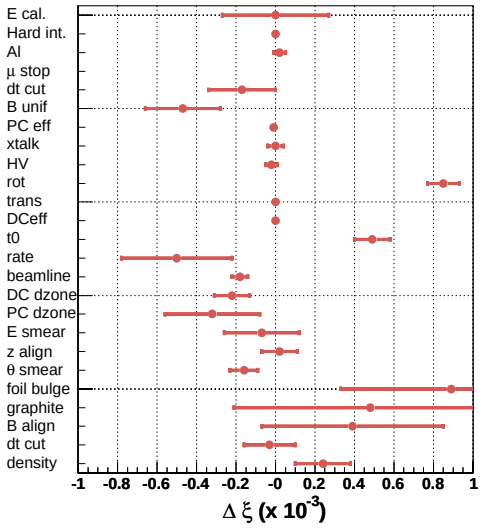

Figure 19: Systematic uncertainties for ξ in units of 10^{-3}.

The total projected uncertainty for ρ from the terms in Table 4 is 0.25, which is slighty larger than the target value of 0.21. A similar analysis can be performed for δ. The target uncertainty is 0.28 and the contribution from the theoretical uncertainty is 0.10. The projection in the Table is 0.30, which is close to the target value. The situation for ξ is more speculative. Using the 2002 data the systematic uncertainties for ξ can be evaluated. The terms that were examined for ρ and δ are displayed in Fig. 19. The term for the uncertainty in the target thickness, labeled "graphite", will disappear as the thickness of the Al target is known precisely. The systematic for the μ stop term is off scale. There are additional terms that are important for ξ, which are listed in the last lines of Table 4.

The target uncertainty for ξ is 0.7. The same arguments that apply to projected reductions in systematic uncertainties for ρ and δ also apply to the same terms for ξ. The leading systematic in this case is due to muons stopping ahead of the target, which was not handled properly in the MC for 2002. This term will be reduced by a factor of $\sim$2 because of reduced differential depolarization between the gas and the target, by another factor of 2 by reducing the fraction stopping in the gas, and by a factor of 10 by including the depolarization in the MC. An improved OPERA map will be required to reduce the contribution from B field distortion. The entry for the fringe field assumes that the depolarization is 0.3% and is simulated in the MC with accuracy of 10%. If the listed goals are met, the quadratic sum of the terms shown is 0.61, which is very encouraging.

6.3 Systematics for the future of $\mathcal{TWIST}$

To reach the final goals of a factor of ten reduction in total error from the previously published results requires achieving the target values for the systematic uncertainties given in Table 3. The goal for ρ cannot be met without reducing the contributions from the uncertainty in η and from theoretical radiative corrections. For example, if the precision on η is improved at some later time with the $\mathcal{TWIST}$ apparatus or by an experiment at PSI, the value of ρ can be recomputed and the error on ρ can be reduced. After excluding these two terms and the analogous term for the theoretical radiative corrections for δ, the projected systematic uncertainties for 2004-2005 are almost good enough for the final results. One challenge will be to keep the driving terms under control over a much longer data collection period.

In contrast to ρ and δ, the 2004-2005 run will be our first measurement of $\mathcal{P}_\mu\xi$. It will provide the crucial experience necessary to identify the $\mathcal{P}_\mu\xi$-specific limiting effects that require further effort to achieve the ultimate reduction in systematic uncertainties anticipated in Table 3.

The question is often asked whether $\mathcal{TWIST}$ will measure η. A new improved measurement of η is extremely important, as it is sensitive to the scalar sector. It is also necessary to remove a limitation on the extraction of the Fermi coupling constant G_F from improved muon decay lifetime measurements. The PSI experiment [5] has stated goals which are probably beyond the reach of $\mathcal{TWIST}$, as one would expect for an experiment designed with its measurement in mind. $\mathcal{TWIST}$, on the other hand, is not ideally suited to measuring η. As we operate it now, at 2 T, the momentum range which is most sensitive to η is problematic due to the pitch ambiguity of our chamber spacing. On the other hand, by lowering the field , this can be solved at the expense of higher momentum coverage, and the major problems are expected to be positron interaction uncertainties. At a lower average field, the homogeneity suffers due to saturation effects in the yoke, and at the very least an appropriate field map would have to be obtained and simulated with OPERA. While η has not been a priority for $\mathcal{TWIST}$, we are certainly aware that effort on η would be well justified in any case, but especially if the PSI experiment cannot achieve its stated goal.

Of course, there will be incremental improvements in reducing systematics by concentrating on the leading terms. In particular, the dominant uncertainty for ρ and δ will be the positron interactions systematic. This is not a surprise; it is the place where the data confronts the Monte Carlo most directly. Furthermore, we have the least direct experimental test on it, so it ends up being explored indirectly. To adequately reduce this systematic, we are going to need abundant amounts of upstream and downstream stops to tune and validate our GEANT simulation, and careful tuning of the fiducial regions to minimize the sensitivity for each parameter individually. Different fiducial regions are needed because for ρ, we care about the interactions and the absolute response of the spectrometer while for ξ and δ, we care about the interactions and the relative upstream/downstream response of the spectrometer. All parameters will be optimized by measurements where the interactions are minimal; that means extending to larger $|\cos\theta|$, which of course will also aid in statistics for ξ and δ (see below). In contrast, reducing the lower $|\cos\theta|$ boundary will achieve very little, if anything. We can probably also improve the situation for all the parameters by raising the p_{tot} and p_T upper limits as practical.

Concerning the $|p_z|$ constraint, it was set at 13.7 MeV/c for the 2002 data analysis. For ρ, that was too low. It avoided the longitudinal periodicity of the spectrometer, but not 1.5 times the longitudinal wavelength, which still ends up being a problematic area. We should perhaps have limited the ρ analysis to $|p_z| > 20$ MeV/c. Doing so would also reduce $\Delta\rho/\Delta\eta$ somewhat, thus providing a small reduction in the η systematic which is eventually going to become important. In contrast, for ξ and δ we probably would have optimized our result by setting the $|p_z|$ cut lower! The longitudinal wavelength problem should not be an issue for the muon decay asymmetry as long as the upstream and downstream detector halves respond similarly. A lower $|p_z|$ cut, coupled with a larger $|\cos\theta|$ upper limit, will probably necessitate the addition of a minimum p_T cut, but that should not be difficult. Decreasing the minimum $|p_z|$ cut will decrease the correlation between $\mathcal{P}_\mu\xi$ and $\mathcal{P}_\mu\xi\delta$. If so, it will also increase the correlation between $\mathcal{P}_\mu\xi$ and δ beyond the present value of $\sim$0.55.

Improvements are planned in essentially all areas to control or reduce systematics. Many of these have been discussed earlier in the document and are summarized here according to the category of systematics.

- *Chamber response:* During data collection, the differential pressure will be monitored to keep the foil positions stable with little if any bulge (the former is more important than latter). The full dense stack has been instrumented to improve the fiducial region. At present, limited validation

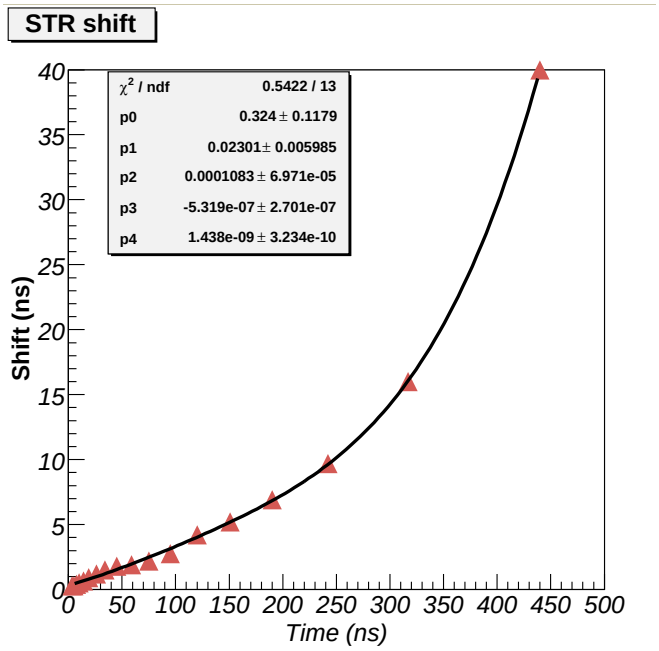

Figure 20: Preliminary comparison of STRs obtained from Garfield simulation to STRs from straight line fits to data.

of the STRs used from Garfield , as indicated in Fig. 20, point to agreement at the 4% level at 100 ns growing to 10% at 400 ns drift time. The first guess and helix fitter is being upgraded to use plane-dependent STRs. Garfield STRs will be replaced by STRs obtained from the data which track variations in the density.

Simulation of wire inefficiencies following a muon hit has been implemented. This inefficiency has been measured for the highly ionizing muons in the chamber nearest the target. For the 2002 analysis this simulation was only used to estimate a systematic uncertainty. Further work is needed to extrapolate to the less ionizing parts of the muon trajectory. Including this effect in the base simulation will clearly increase the scale factor in the systematic estimation. This will not be a limiting systematic.

- *Stopping target thickness:* The Al target now in use has a known thickness, which eliminates a problem we had with the Mylar target.
- *Positron interactions:* Adequate statistics will be taken with muons stopping upstream to validate GEANT. In addition, data will be taken with a higher momentum cloud beam to provide downstream stops, probably using a relatively thin Mylar stopping foil at the exit of the detector stack. Improved online monitoring and semi-online data analysis will permit fast identification of run-to-run differences. The addition of a downstream beam package for symmetry with the upstream will be used for some data sets. Improvements to the tracking that relate to this topic include allowing for kinks in modules without hits and enabling energy loss in the tracker. A detailed examination of measured kinks in data *vs* MC may be informative. While we are considering switching to a maximum likelihood fit to simplify the weighting of individual hits according to individual position precisions, it also makes it possible to deal with kinks more readily. A review of the accuracy of the geometry and adding beam e^+ and beam π^+ in the simulation trigger are also on the list. Work continues on GEANT4 as a possible replacement for GEANT3.
- *Spectrometer alignment:* The alignment of the chambers with respect to the magnetic field map may be sensitively determined by measuring the deviation of the positron tracks from a helix structure. The estimated uncertainty from this procedure is 2%. The presently-implemented

calibration code is sufficiently flexible that this rotation can be incorporated as a change to the alignment calibration files which does not alter the relative positions of the chamber planes. This procedure should increase the scaling factor for that systematic by ∼50, so it will be well under control.

- *Momentum calibration:* The adequacy of the OPERA map for 2.00 T will be reviewed and explicit OPERA maps for 1.96 T and 2.04 T are needed. The energy calibration algorithm will be improved, including breaking the correlation between parameters. The present tracking code relies on a gaussian approximation for weighting the kinks used in the treatment of multiple scattering. It also uses a resolution function averaged over all cell positions. We are working on a maximum likelihood helix fitter to implement proper Landau distributions for the multiple scattering, as well as a position-dependent resolution weighting. These developments will improve the endpoint fits and increase the reliability of our treatment of the multiple scattering.

- *Track selection algorithm:* Improvements in the algorithms are planned, including better use of the muon stopping position uv coordinate.

- *Muon beam stability:* Feedback to the gas degrader setting will be implemented to stabilize the mean muon stopping position in z. The TEC provides a major upgrade to the beam characterization capabilities, including the possibility of including position dependence of the momentum. A graphite production target is now in use, which provides a smaller source, higher luminosity, lower Z, reduced secondary sources, and less sensitivity to proton beam position. Also on the list is to verify and exploit GEANT-based simulations of the surface muon production mechanism in the primary production target (T1GEANT) and of the transport of muons in the secondary beam line (M13GEANT).

6.4 Computational requirements

Processing the $\mathcal{TWIST}$ data requires extensive computing resources. Production generation of Monte Carlo data and analysis of both MC and real data to obtain the results presented in Section 5 was done between late May and early October 2004 on the WestGrid UBC/TRIUMF cluster. This cluster consists of 504 dual 3 GHz Xeon nodes. During this period $\mathcal{TWIST}$ used a total of 20,000 CPU days or an average of 15% of the resources. At present, it takes 0.73 CPU days to generate 10^6 MC events and 0.42 CPU day to analyse these events. In the case of real data, it takes 0.5 CPU days to analyse 10^6 events. Some of the data sets have to be analysed more than once for systematics studies using varying input parameters.

Although the MC generation and analysis software will be improved, few of the changes proposed are expected to add any significant calculation time to the processing. Using the above numbers, the statistical requirements outlined in Section 6.2 and the experience gained during the last six months of analysis, we can predict the computational requirements to produce a result for the 2004-2005 data taking period. We expect to use some 6,000 CPU days to generate MC data, 6000 CPU days to analyse it and 7,000 CPU days to analyse the real data for a total of 19,000 CPU days.

For the final, high statistics data taking period, the estimates for processing the data are 30,000 for MC generation, 30,000 for MC data analysis and 40,000 for real data analysis, adding up to a total of 100,000 CPU days.

The WestGrid UBC/TRIUMF cluster is at this moment procuring another 504 nodes for a doubling of the resources. Assuming we will need some 30,000 CPU days (150% of the calculated needs) to extract the next set of results from the 2004-2005 data, this can be accomplished by using on average 6% of the Westgrid upgraded resources until the end of 2005. Processing of the final data will take place in 2006-2007 and could still be accomodated by WestGrid with a usage of 10% of the resources (assuming resources would still be only at the level of 2005). The WestGrid consortium has already started planning a request for the future CFI competition. Also, the TRIUMF/Atlas Data Analysis Hub should start operation by 2006, where 20% of the resources are targetted for users other than Atlas. With these prospects, there should be no problem finding the needed cycles to process the TWIST data in due time.

7 Summary

This Research Proposal has outlined in detail the accomplishments of the $\mathcal{TWIST}$ group so far, and has described a realistic way for the project to proceed toward its eventual goals of improvement of ρ and δ by at least an order of magnitude, and twice that for $\mathcal{P}_\mu\xi$, compared to previous experiments. We have an excellent team in place, and with adequate resources we feel that our goals can be accomplished in a timely way.

Our milestones have already been implied, but it is important to summarize them here. We are in a position to make our first direct measurement of $\mathcal{P}_\mu\xi$, with an ambitious goal of increasing the precision by a factor of approximately eight compared to previous direct measurements [19]. Data collection is starting in Fall 2004, and should be completed by May 2005 at the latest. Analysis can be expected for this data set in the third quarter of 2005. The same analysis will yield new values for ρ and δ which eclipse our recently submitted values by a factor of two.

The final stages of the $\mathcal{TWIST}$ program for these parameters will require much more work. An improved field map may be necessary, and in order to achieve our greatest physics potential, we will need input from our theoretical colleagues regarding radiative corrections. The map can be performed in about a month, and will be part of the program for 2005. By late 2005, we expect to have all necessary developments in place to give us the best quality muon beam possible, including a new design of graphite target from TRIUMF. Also by that time, all software development described in this proposal will be complete. As a byproduct of our systematics assessments, we will also be able to provide the most detailed verification of GEANT simulations for positron interactions in the range of tens of MeV.

We will also want to investigate the potential for $\mathcal{TWIST}$ to improve the uncertainties in η. This will require a dedicated amount of beam time and simulation, just to assess the feasibility, but as our understanding of the detector improves, it could provide a very appealing physics possibility.

To follow this timeline, adequate, stable, and longer-term funding is essential to keep our team of experts in place. $\mathcal{TWIST}$ has taken a long time to get to this stage, but it is now a proven set of hardware, software, and people, who simply need continued support to produce excellent results.

References

[1] L. Michel, Proc. Phys. Soc. **A63**, 514 (1950).

[2] W. Fetscher, H.-J. Gerber, and K. F. Johnson, Phys. Lett. **B173**, 102 (1986).

[3] TWIST Collaboration, J. R. Musser *et al.*, arXiv:hep-ex/0409063 (TRI-PP-04-21), submitted to Phys. Rev. Lett., 2004.

[4] TWIST Collaboration, A. Gaponenko *et al.*, arXiv:hep-ex/0410045 (TRI-PP-04-22), submitted to Phys. Rev. Lett., 2004.

[5] W. Fetscher, http://www.cap.bnl.gov/nufact03/WG2/6june/fetscher.pdf, NuFact03, New York, 2003.

[6] S. Eidelman *et al.*, Phys. Lett. **B592**, 1 (2004).

[7] C. Bouchiat and L. Michel, Phys. Rev. **106**, 170 (1957).

[8] A. Sirlin, Phys. Rev. **108**, 844 (1957).

[9] A. B. Arbuzov, Phys. Lett. **B524**, 99 (2002).

[10] A. Arbuzov, A. Czarnecki, and A. Gaponenko, Phys. Rev. **D65**, 113006 (2002).

[11] A. Arbuzov and K. Melnikov, Phys. Rev. **D66**, 093003 (2002).

[12] M. V. Chizhov, arXiv:hep-ph/0405073, 2004.

[13] R. L. Henderson *et al.*, arXiv:hep-ex/0409066 (TRI-PP-04-20), submitted to Nucl. Instr. and Meth., 2004.

[14] A. Jodidio *et al.*, Phys. Rev. **D34**, 1967 (1986).

[15] A. Jodidio *et al.*, Phys. Rev. **D37**, 237 (1988).

[16] D. G. Fleming and M. Senba, Atomic Physics with Positrons, ed. J.W. Humberston and E.A.G. Armour, Plenum, 1987.

[17] F. James, Nucl. Instr. and Meth. **211**, 45 (1983).

[18] G. Lutz, Nucl. Instr. and Meth. **A273**, 349 (1988).

[19] I. Beltrami *et al.*, Phys. Lett. **B194**, 326 (1987).